Development of heteroarm star polymer for antithrombogenic and antimicrobial coating materials

Masayasu Totani

2014

Graduate School of Materials Science
Nara Institute of Science and Technology

CONTENTS

CONTENTS

GENEAL INTRODUCTION

GENEAL INTRODUCTION

1. Problems of artificial organs

Biomaterials in the form of implants (sutures, bone plates, joint replacements, ligaments, vascular vessels, heart valves, intraocular lenses, dental implants, etc.) and medical devices (pacemakers, biosensors, artificial hearts, blood tubes, etc.) are widely used to replace and/or restore the function of traumatized or degenerated tissues or organs, to assist in healing, to improve function, to correct abnormalities, and thus improve the quality of life of the patients [1].

To this day, the various materials used in biomedical applications may be grouped in to (a) metals, (b) ceramics, (c) polymers, and (d) composites made from various combinations of (a), (b) and (c) (Figure 1) [1].

In essence, biomedical materials are prone to adhesion of proteins, cells, and bacteria, which causes functional failures in implants, artificial organs, catheters, and diagnostic devices and increases the risk of secondary infections [2,3]. See Sections 3 and 4 for further details. Good antithrombogenicity and antimicrobial activity are essential for artificial organs, which are used in direct contact with blood.

2. The background of this study

I aim to develop a new designed synthetic coating material for small diameter artificial blood vessels, blood tubes and catheters (Figure 2).

Ramakrishna et al. reported as follows the review of polymer-composite materials for biomaterials application. Blood vessels after autologous transplantation are used to replace segments of the natural cardiovascular system (mainly successful in the case of blood vessels with internal diameter of over 5 mm) that are diseased or closed (atherosclerosis, deposits on the inner surface of the vessels restricting the flow of blood and increasing blood pressure). Most widely used artificial vascular vessels are woven or knitted fabric tubes of PET material or porous tubes of extended PTFE and PU materials. The most important property of the artificial vascular vessel is their porosity. Most of artificial vascular vessels need preclotting prior to transplantation to minimize blood leakage. In another approach, the artificial vascular vessels are impregnated with collagen or gelatin to seal the pores and also to improve the dimensional stability of artificial blood vessels (These are known as composite vessels). PET (Dacron) vascular vessels (woven or knitted fabric tubes) are mainly successful in the replacement of large diameter blood vessels (12-38 mm diameter). A major issue for artificial vascular vessels is the reaction between the surface of the material and blood that can cause destruction of blood cells and thrombus formation. See Sections 3 for further details. On the other hand, it is well known that blood coagulation on foreign surface is primarily triggered by the activation of factor XII (FXII). The activation FXII convert plasma prekallikrein (PK) to kallikrein (KAL), and subsequently KAL converts high molecular weight kininogen (HMW-kg) to kinnins. Finally, PK is consumed by conversion to KAL in the initial stage of coagulation, and fibrinogen and FXII are consumed by conversion to fibrin and activated factor XIII (FXIIIa) in the final stage of coagulation (Figure 3) [4].

Biocompatibility of PET fibers and fabrics is generally considered to be

acceptable. Protein adsorption and platelet adhesion of vascular vessel inner surface of PET are occurred, and form clots. Fortunately, endothelial cells can migrate along this thrombus layer as a scaffold, and then the cells formed the pseudointima which is inner endothelium-like layer of blood vessels. Therefore, a large diameter vascular vessel can improve patency for a long time.

In addition, vascular vessels made from PET fabric are excellent at strength and flexibility, and are able to be cut easily into the proper length and be sutured at the surgery. For these reasons, PET vascular vessels are mainly used even now.

Expanded PTFE (e-PTFE or GoreTex) is widely used for medium diameter (6-12 mm) vascular vessels. The porous non-woven microstructure of e-PTFE provides vascular vessels with a mechanical behavior matching to that of the host blood vessels compared to the vascular vessels made of non-porous (solid) materials. Moreover, the inner (luminal) surface of e-PTFE vessels facilitates formation of neointima (newly formed endothelial tissue lining) that avoid the complications such as formation of thrombi (blood clot) and emboli (dislodged blood clot). However, the exact mechanisms of neointima formation are not clear.

As described above, artificial vascular vessels cause thrombus formation on the inner surface. Protein adsorption on the material surface is considered to initiate thrombus formation. In fact, the protein adsorption property of small diameter artificial vascular vessels is not yet good enough for the demanding application. So, there is strong need for developing a highly blood compatible material that can construct a vascular vessels itself or a facile method to give resistance to thrombus formation to the surface of the vascular vessels by modification. It has been reported that the surface coated with hydrophilic polymers can inhibit or reduce platelet adhesion.

3. Study of antithrombogenic and antimicrobial materials

As described previously, vascular vessels of PET or PTFE has problem that forms clots after the implantation. Therefore, many antithrombogenic materials for the vascular graft have been studied (Table). Coating with collagen and gelatin was performed to promote pseudo-endothelium layer formation in the large diameter artificial vessels. However, this methods can not be applied to the small diameter artificial vessels because of the embolization at the early stage. Therefore, further studies for more surpassing antithrombogenic maerials, such as microdomain phase-separation structure [5] and MPC polymer [6,7], have been developed (Figure 3).

A common strategy to prevent protein and microbial adhesion is to modify such material surfaces by hydrophilic polymers including non-ionic poly(ethylene glycol) (PEG) [8-10], poly(2-hydroxyethyl methacrylate) (PHEMA), PHEMA-styrene block copolymer (PHEMA-PSt-PHEMA) [5], poly(2-methoxyethyl acrylate) (PMEA) [11], polyethylene oxide-polypropyleneoxide block copolymer (PEO-PPO-PEO) [12,13] and PEO star-shaped polymers [14,15]. Recently, zwitter ionic polymers including poly(2-methacryloyloxyethyl phosphorylcholine) [6,7], poly(sulfobetaine methacrylate) [16] and poly(carboxybetaine methacrylate) [17] have been utilized as new materials (Figure 4). These polymers on surfaces prevent the non-specific hydrophobic binding of proteins, cells and bacteria, which is the primary divining force in the initial stage of the adhesion mechanism. Polymer chains anchored on surfaces also provide physical barriers against protein adhesion due to the exclusion volume around polymer chains

[18,19]. These polymer effects of hydrophilic layers and exclusion volumes are further enhanced when polymer chains are densely packed and form brush structures on surfaces (Figure. 1) [20,21]. A common method to prepare polymer brushes is polymerization of monomers from initiators which are covalently fixed on surfaces (graft polymerization) [20] (Figure 3). Another method is to covalently attach pre-existing polymer chains onto the plastic surfaces [13]. Although polymer brushes can be prepared by these methods, achieving a high density of polymer brushes on plastics is very challenging because chemically inert plastic surfaces are difficult to covalently modify with a high density of initiators or attached with pre-existing polymers, and the number of reaction sites is also limited. In addition, the modification of plastic surfaces needs substrate specific chemical treatment, and some organic solvents/agents for surface chemistries and polymerization may not be compatible with existing biomedical plastics. Therefore, a simple and versatile method to prepare high-density polymer brush coatings compatible with biomedical synthetic materials would be beneficial for biomedical applications.

4. Star polymers in living polymerization

Recently, living radical polymerization (LRP) including metal-catalyzed LRP (ruthenium, iron complex, etc.) and atom transfer radical polymerization (copper complex), living anionic or cationic polymerizations have been many developments in various researches area. These polymerizations can be used for the preparation of copolymers, incorporating a broad spectrum of radically (co)polymerization monomers

forming materials with predetermined molecular weight, and narrow molecular weight distribution (Figure 4). It can be used to create polymers with precise molecular weights and controlled architectures such as block copolymer, random copolymer, grafted copolymer, star polymers and polymer brush (Figure 5).

Synthesis of well-defined microgel star polymers with metal-catalyzed LRP have synthesized by the arm-first method via a polymer-linking process with a bifunctional alkene (a linking agent). A remarkably simple method for manipulating the topologies of functional star and heteroarm star copolymers by using the LRP and indicated an easier and more efficient strategy to synthesize functional star polymers with controlled structures [22-24].

5. The aim of this study

In this thesis, I demonstrate a new design strategy to prepare high-density stable coatings of hydrophilic polymer chains on plastic surfaces. I utilize star-shaped polymers pre-assembled with a number of hydrophilic PHEMA polymer chains. This star-polymer architecture intrinsically provides high polymer chain density when coated on surfaces (Figure 6). The star polymers are tightly packed with the highly entangled polymer chains, providing physical cross-linking of star polymers, and increasing coating stability. This method allows for a simple coating method of solvent casting or dip coating on pre-existing plastic materials, which minimizes the use of organic solvents and chemical treatment, facilitating coating preparation. In addition, I further extended the polymer design to include heteroarm star polymers having both

hydrophilic PHEMA and hydrophobic poly(methyl methacrylate) (PMMA) polymer chains. In general, PMMA has higher hydrophobicity, hardness, and adhesiveness to plastic surfaces, as compared to PHEMA [24]. Therefore, I expect that the star-polymer PMMA arms will anchor the hydrophilic PHEMA chains onto plastic surfaces, increasing the stability of polymer coatings in water, and physical durability.

In this study, I synthesized mono-dispersed star-polymer architectures using a living radical polymerization method [26]. The surface structures and morphologies of the polymer coatings were examined by SEM and AFM. The mechanical stability of coatings was also examined by quantifying the resistance of coatings against physical scratching. The anti-adhesion activity of star polymer coatings was determined using platelets and model bacterium *E. coli* (Figure 7). The anti-adhesion property of coatings was also examined for coating stability after soaking them in buffer or surfactant solution for 7 days to assess.

6. References

[1] Ramakrishna S, Mayer J, Wintermantel E, Leong KW. Biomadical applications of polymer-composite materials: a review. Compos Sci Technol 2001;61:1189-224.

[2] Darouiche RO. Treatment of infection associated with surgical implant. N Engl Med 2004;350:422-29.

[3] Mack D, Davies AP, Harris LG, Rohde H, Hostkotte MA, Knobloch JK-M. Microbial interactions in staphylococcus epidermids biofilms. Anal Bioanal Chem 2007;387:399-408.

[4] Zhang Z, Wang J, Tu Q, Nie N, Sha J, Liu W, Liu R, Zhang Y, Wang. J Surface modification of PDMS by surface-initiated atom transfer radical polymerization of water-soluble dendronized PEG methacrylate. Colloids Surf B 2011;88:85-92.

[5] Shimada M, Unoki M, Inaba N, Tahara H, Shinohara I, Okano T, Sakurai Y, Kataoka K. Effect of adsorbed protein on the adhesion behaviour of platelet to the microdomain surface of 2-hydroxyethyl methacrylate-stylene block copolymer. Eur Polym J 1983;19:929-33.

[6] Iwasaki Y, Ishihara K. Phosphorylcholine-containing polymers for biomedical applications. Anal Bioanal Chem 2005;381:534-46.

[7] Seo JH, Kakinoki S, Inoue Y, Nam K, Yamaoka T, Ishihara K, Kishida A, Yui N. The significance of hydrated surface molecular mobility in the control of the morphology of adhering fibroblasts. Biomaterials 2013;34:3206-14.

[8] Nagaoka S, Nakao A. Clinical application of antithrombogenic hydrogel with long poly(ethylene oxide)chains. Biomaterials 1990;11:119-21.

[9] Nakao A, Nagaoka S, Mori Y. Clinical application of antithrombogenic hydrogel with long poly(ethylene oxide) chains. J biomater app 1987;2:219-34

[10] Banerjee I, Pangule RC, Kane RS. Antifourling coatings: Recent developments in the design of surfaces that prevent fouling by protein, bacteria, and marine organisms. Adv Mater 2011;23:690-718.

[11] Tanaka M, Motomura T, Kawada M, Anzai T, Kasori Y, Shiroya T, Shimura K, Onishi M, Mochizuki A. Blood compatibility aspects of poly(2-methoxyethyl acrylate) (PMEA)- relationship between protein adsorption and platelet adhesion on PMEA surface. Biomaterials 2000;21:1471-81.

[12] Lee JH, Ju YM, Kim DM. Platelet adhesion onto segmented polyurethane films surfaces modified by addition and croslinking of PEO-containing block copolymers. Biomaterials 2000;21:683-91.

[13] Nejadnik MR, van der Mei HC, Norde W, Busscher HJ. Bacterial adhesion and growth on a polymer brush-coating. Biomaterials 2008;29:4117-21.

[14] Sofia SJ, Premnath V, Merrill EW. Poly(ethylene oxide) grafted to silicon surface: grafting density and protein adsorption. Macromolecules 1998;31:3059-70.

[15] Gasteier P, Reska A, Schulte P, Salber J, Offenhausser A, Moeller M, Groll J. Surface grafting of PEO-based star-shaped molecules for bioanalytical and biomedial applications. Macromol Biosci 2007;7:1010-23.

[16] Cheng G, Zhang Z, Chen S, Bryers JD, Jiang S. Inhibition of bacterial adhesion and biofilm formation on zwitterionic surfaces. Biomaterials 2007;28:4192-9.

[17] Cheng G, Li G, Xue H, Chen S, Bryers JD, Jiang S. Zwitterionic carboxybetaine polymer surfaces and their resistance to long-term biofilm formation. Biomaterials 2009;30:5234-40.

[18] Ayres N. Polymer brushes: applications in biomaterials and nanotechnology. Polym Chem 2010;1:769-77.

[19] Chen S, Li L, Zhao C, Zheng J. Surface hydration: Principles and applications toward low-fouling/nonfouling biomaterials. Polymer 2010;51:5283-93.

[20] Yoshikawa C, Goto A, Tsujii Y, Fukuda T, Kimura T, Yamamoto K, Kishida. Protein repellency of well-defined concentrated poly(2-hydroxyethyl methacrylate) brushes by size-exculusion effect. Macromolecules 2006;39:2284-90.

[21] Llanos GR, Sefton MV. Does polyethylene oxide possess a low thrombogenicity. J Biomater Sci Polymer Edn 1993;4:381-400.

[22] Kamigaito M. Recent developments in metal-catalyzed living radical polymerization. Polym Journal 2011;43:105-120.

[23] Hadjichristidis N. Synthesis of miktoarm star polymers. J polym Sci Part A 1999;37:857-871.

[24] Shimomoto H, Fukami D, Irita T, Katsukawa K, Nagai T, Kanaoka S, Aoshima S. Synthesis of fluorine-containing star-shaped poly(vinyl ether)s via arm-linking reactions in living cationic polymerization. J polym Sci Part A 2012;50:1547-55.

[25] Bauer S, Schmuki P, Von der Mark K, Park J. Enginnering biocompartible implant surfaces Part I: materials and Surfaces. Prog Mater Sci 2013;58:261-326.

[26] Ouchi M, Terashima T, Sawamoto M. Transition metal-catalyzed living radical polymerization: Toward perfection in catalysis and precision polymer synthesis. Chem Rev 2009;109:4936-5050.

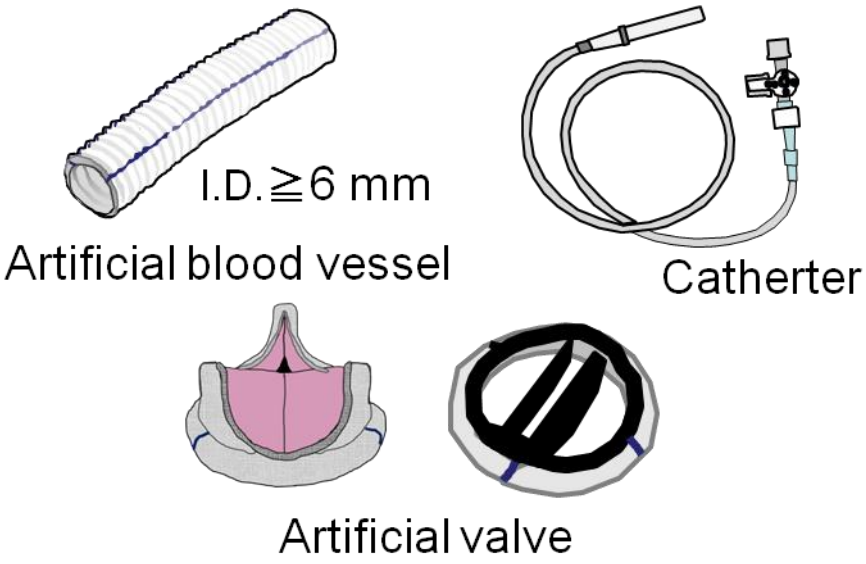

Figure 1. Commercially available artificial organs

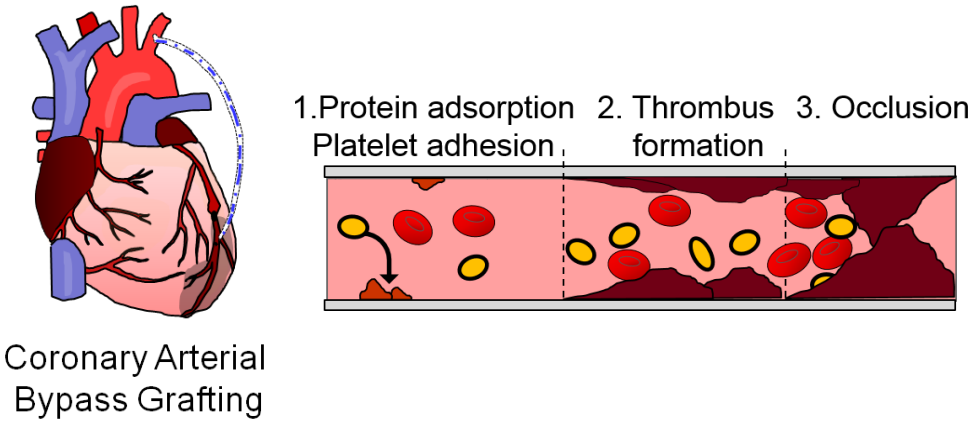

Figure 2. Artificial organs under development and problems of thrombus

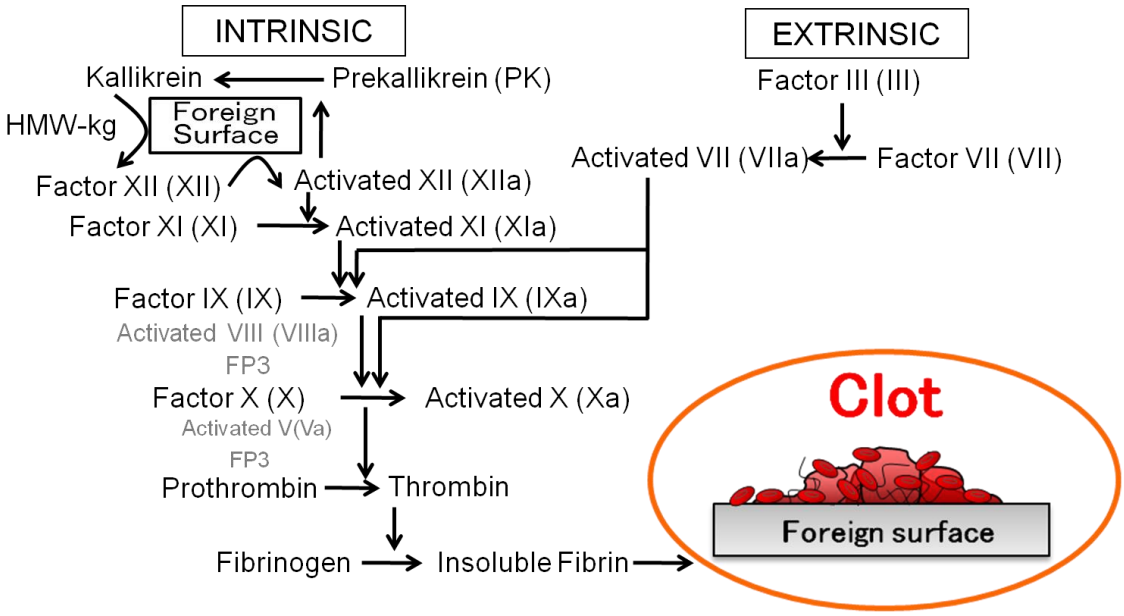

Figure 3. Mechanisms of blood coagulation with activated proteins.

(Figue 9, Nakao et al. [6]).

Table. Antithrombogenic and/or antimicrobial polymers

Polymer	Resisting materials	Substrates	References
Poly(ethylene glycol) (PEG)	protein, platelet	PVC	5-7, 10-13
poly(2-hydroxyethyl methacrylate) (PHEMA)	protein, platelet		8
poly(2-methoxyethyl acrylate) (PMEA)	protein,	PET	9
Poly(2-methacryloyloxyethyl phosphorylcholine) （PMPC）	protein, platelet	PET	14,15
Poly(sulfobetaine methacrylate) (PSBMA)	proteins, platelet bacteria	PET	16
Poly(carboxybetaine methacrylate) (PCBMA)	proteins, platelet bacteria	PET	17

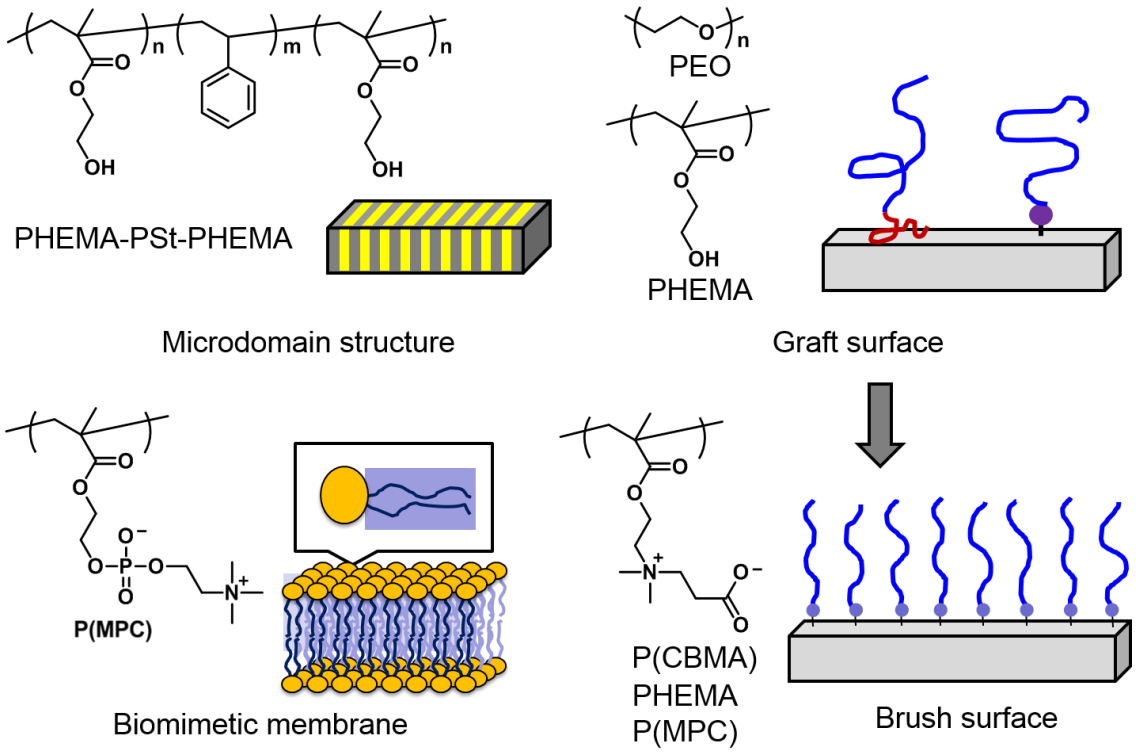

Figure 3. Various biocompartible polymers.

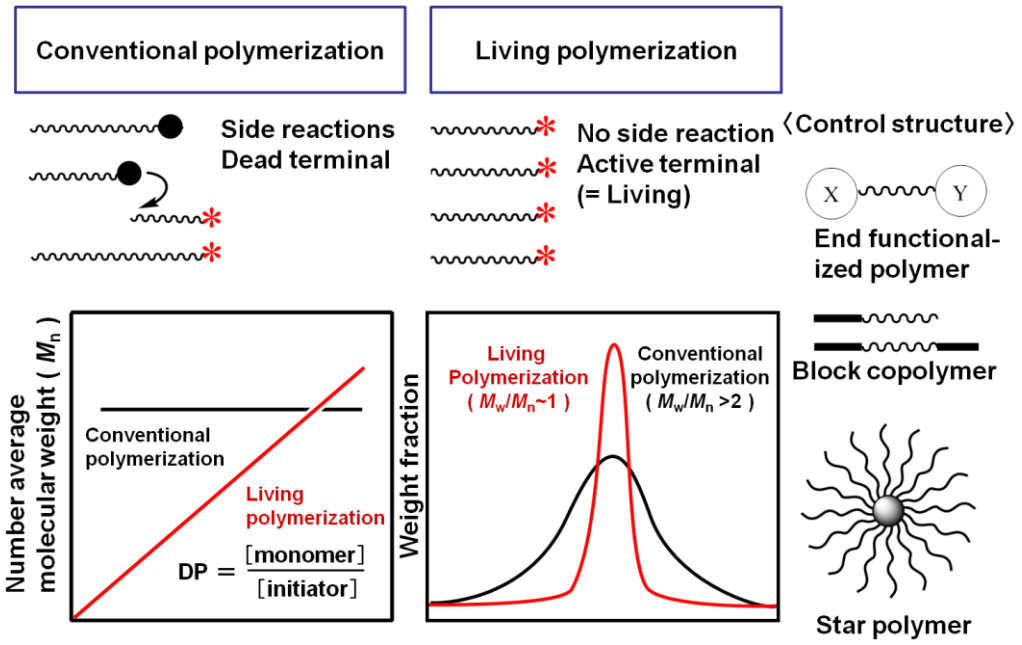

Figure 4. The advantage of living radical polymerization

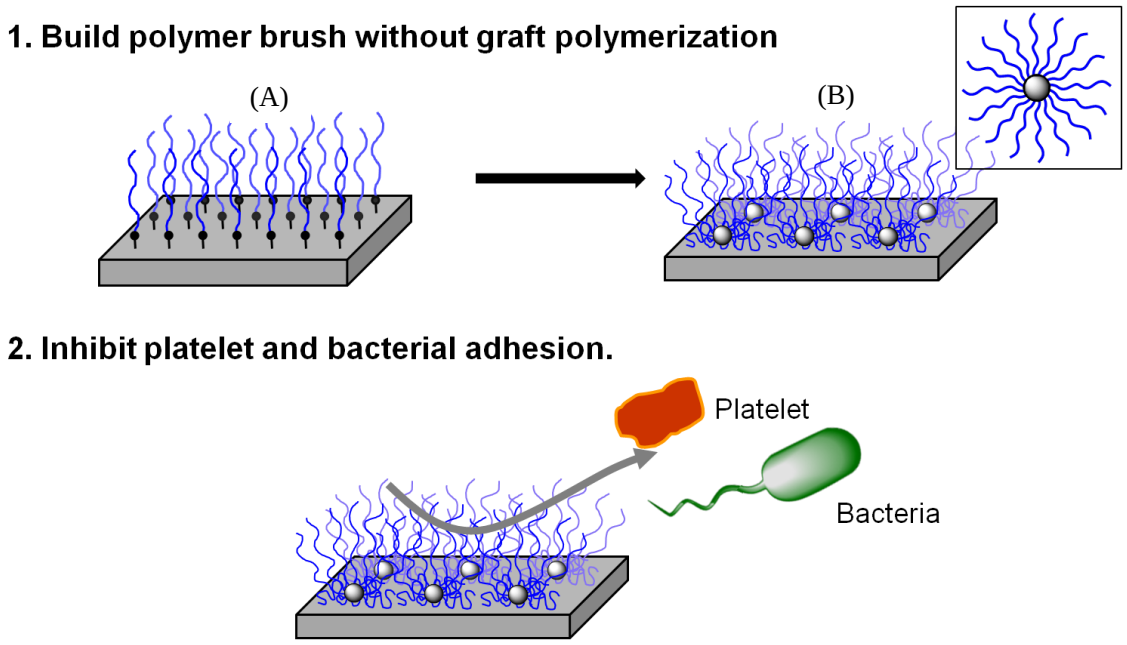

Figure 5. Polymer brush structures on surfaces by (A) graft polymers vs. (B) star polymers.

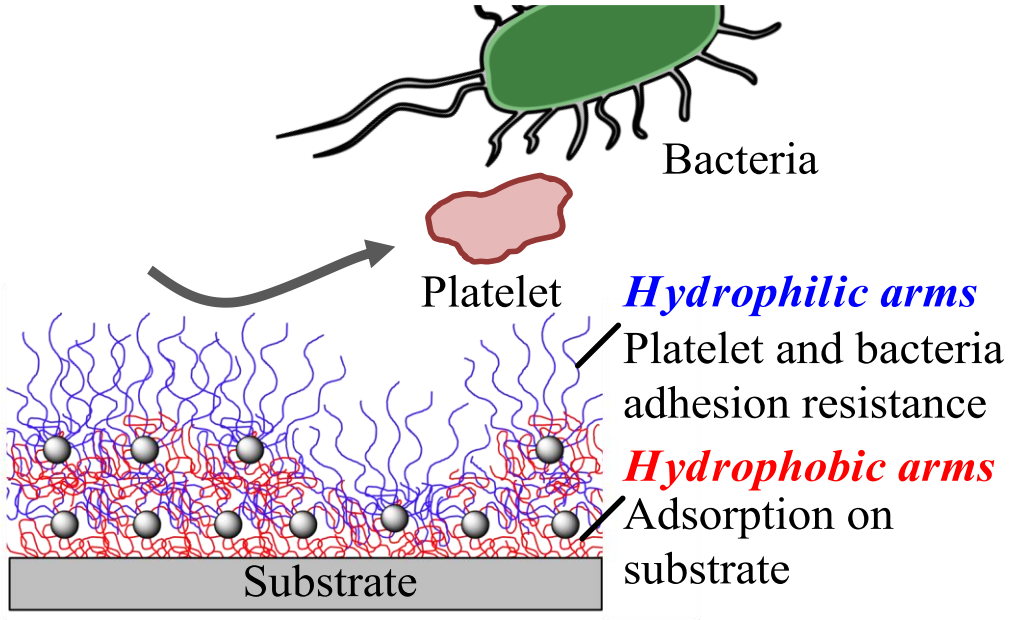

Figure 6. Hydrophilic / hydrophobic heteroarm star polymers coated surface model.

CHAPTER 1

Synthesis of heteroarm star polymers

CHAPTER 1

Synthesis of heteroarm star polymers

1-1. Introduction

Star polymers can be synthesized by living radical polymerization principally in the core-first and arm-first method [1-5]. The arm-first methods is based on linking reaction of linear polymers prepared by the living polymerization upon the addition of the divinyl compounds. This method has now been widely applied to the synthesis of various star polymers because it is facile to form high molecular weight star polymer with large number of arm chains by the addition of divinyl compounds to the living linear polymers [6]. Recently, Beak et al. demonstrated $RuCl_2(PPh3)_3$-catalyzed initiating system to examine the effects of various reaction conditions on the yield, number of arm chains, and gyration radius of star polymers. [7] Terashima et al. reported the new synthetic strategy for star polymers containing metals in the core by direct in situ encapsulation of the catalysts with poly(methyl methacrylate) (PMMA) arms or poly(ethylene glycol) methyl ether methacrylate (PEGMA) arms with this method [8,9]. Thus, Ahmad et al. synthesized Eu(III)-bearing PEG star polymer according to this method [10]. The water soluble star polymer is a promising candidate for biological applications such as bioimaging. Various homoarm star polymers having PMMA and poly(buthyl methacrylate) block or and methyl methacrylate and buthyl methacrylate random copolymer arms can be synthesized using liner pre-polymer as macroinitiator [11]. Many functional star

polymers would be developed for various applications in the future.

In this study, I designed the star polymers having both hydrophilic (antithrombogenic block) and hydrophobic (vessel wall-attaching block) polymers to coat the surface of artificial vascular grafts (Figure 1-1), which can change the surface properties of addition antithrombogenic or antimicrobial. To achieve this purpose, I have synthesized heteroarm star polymers using living radical polymerization of methyl methacrylate (MMA) and 2-(trimethylsilyloxy)ethyl methacrylate (TMSOEMA) were separately polymerized with $Ru(Ind)Cl(PPh_3)_2$ as a catalyst and ethyl α-chloro-α-phenylacetate (ECPA) or methyl α-chloro-α-phenylacetate (MCPA) as an initiator, respectively, to give living PMMA and poly(2-(trimethylsilyloxy)ethyl methacrylate) (PTMSOEMA) with relatively narrow molecular weight distributions (M_w/M_n ~ 1.3) (Scheme 1-1). Ethylene glycol dimethacrylate (EGDMA) was then polymerized by adding to the solution consisting of Ru-catalyst and the living PMMA and PTMSOEMA (mol%/mol% = 75/25, 50/50 and 25/75) as macroinitiators, resulting in heteroarm star polymers with high yields (> 93%) via intra- and inter-linking reaction between living PMMA and PTMSOEMA (Scheme 1-2)

After the trimethylsilyloxy protecting group was removed from PTMSOEMA, resulted PHEMA/PMMA heteroarm star polymers were coated on the PET surfaces. The surface structures and morphologies of the polymer-coated surfaces were examined by scanning electron microscope (SEM) and atomic force microscope (AFM). The mechanical stability of coatings was also examined by quantifying the resistance against mechanical scratching test.

1-2. Materials and Methods

1-2-1. Materials

Methyl methacrylate (MMA) (Tokyo Chemical Industry Co., Ltd., Tokyo (TCI), Japan; purity >99%), tributylamine (*n*-Bu_3N) (TCI; purity >98%), toluene (Aldrich, purity >99%), and EGDMA (Aldrich >98%) were purified by distillation over calcium hydride before use. Chloro(indenyl)bis(triphenylphosphine)ruthenium [Ru(Ind)Cl(PPh_3)$_2$ (Ru), STREM; purity >98%], triethylamine (TCI, purity >98%) were used without purification. Water used in this work was deionized water from a Milli-Q (18 MΩ•cm) system. ECPA, MCPA [12] and 2-(trimethylsilyloxy)ethyl methacrylate (TMSOEMA) [13] were prepared according to the literature. PET film (FS2000, Futamura Kagaku K.K., Osaka, Japan) was cleaned by sonication in 0.2 μm-filtrated ethanol for 30 min, and then dried overnight under vacuum.

1-2-2. Polymer characterization

The M_n, M_w, and molecular weight distribution (M_w/M_n) of the polymers were measured by size exclusion chromatography (SEC) in *N*,*N*-dimethylformamide (DMF) containing 10 mM LiBr at 40 °C (flow rate: 1 mL/min) on three linear-type poly(2-hydroxyethyl

methacrylate) gel columns (Shodex® OHpak SB-806M × 3, exclusion limit = 2×10^7; 0.8 cm i.d. × 30 cm) that were connected to a Jasco PU-2080 precision pump, a Jasco RI-2031 refractive index detector, and a Jasco UV-2075 UV/vis detector set at 270 nm. The M_n and M_w were determined by a calibration curve prepared by 10 standard PMMA samples. ^{1}H nuclear magnetic resonance (^{1}H NMR) spectra of each sample were measured using a JNM-ECP 500 spectrometer (JEOL Ltd, Tokyo, Japan). The absolute M_w and M_w/M_n of the star polymers were determined by multiangle laser light scattering (MALLS) in DMF containing 10 mM LiBr at 40 °C (flow rate: 1 mL/min) on a Dawn E instrument (Wyatt Technology Corp., Ga-As laser, λ = 690 nm). The concentration of residual ruthenium in the star polymers was measured by Microwave-induced plasma mass spectra (MIP-MS) (P-6000, HITACHI, Tokyo, Japan). The hydrodynamic diameter of the star polymers was measured by a dynamic light scattering (DLS) spectrometer equipped with a He–Ne laser at 633 nm (Zetasizer Nano-ZS, Malvern).

1-2-3. Synthesis of precursor polymers (Arms of star polymer)

1-2-3-1. Precursor PMMA (lin-PMMA 10k)

MMA were preliminarily polymerized with 9 mL scale for determining of polymerization behavior by analysis of sampling solution. According to this result, precursor PMMA was synthesized as follows.

Polymerization of MMA was carried out under argon in a 1000 mL round bottom flask equipped with a three-way stopcock. ECPA (4.46 mL, 26.0 mmol), MMA (278.1 mL, 2600 mmol), *n*-Bu_3N solution (30.6 mL, 26.0 mmol, 850 mM in toluene), and $Ru(Ind)Cl(PPh_3)_2$ (2.24 g, 2.60 mmol) were added into toluene (334.6 mL). Immediately after mixing, the polymer solution was separated in nine aliquots into the 100 mL flask at 25°C under argon. The polymer solution was then degassed by Ar bubbling for 10 min. The mixtures were placed in an oil bath with temperature controlled at 80 ºC. The polymerization was terminated by cooling the mixtures in an ice bath after 19 h. The monomer conversion was determined by ^{1}H NMR analysis, the solvent was removed under reduced pressure, and the crude polymer was precipitated in hexane to remove unreacted monomers. The Ru-complex was removed by silica-gel and alumina column chromatography eluted with toluene. After removing the solvent, the resultant PMMA was dissolved in 1,4-dioxane, and lyophilized to give a white powder. M_n = 8,300, M_w = 10,400, M_w/M_n = 1.25 (SEC). ^{1}H NMR (500.16 MHz, $CDCl_3$, $Si(CH_3)_4$ = 0 ppm): δ (ppm) = 4.21-3.94 (-O-CH_2-CH_3), 3.80-3.42 (-OCH_3), 2.22-1.34 (-CH_2-), 1.32-0.64 (-CH_3).

1-2-3-2. Precursor PTMSOEMA

TMSOEMA were preliminarily polymerized with 20 mL scale for determining of polymerization behavior by analysis of sampling solution. According to this results, precursor PTMSOEMA was synthesized as follows.

The precursor PTMSOEMA was prepared using TMSOEMA by the same procedure

described for PMMA except for removal of unreacted TMSOEMA, where the unreacted TMSOEMA was removed by precipitation of crude PTMSOEMA in MeOH/H_2O (80/20 v/v) mixed solvent. M_n = 16,300, M_w = 21,400, M_w/M_n = 1.31. ^{1}H NMR (500.16 MHz, $CDCl_3$, $Si(CH_3)_4$ = 0 ppm): δ (ppm) = 4.14-3.84 (-C*H*$_2$-CH_2-$OSi(CH_3)_3$), 3.84-3.63 (-CH_2-C*H*$_2$-$OSi(CH_3)_3$), 3.60-3.50 (-C*H*), 2.60-1.43 (-C*H*$_2$-), 2.16-0.56 (-C*H*$_3$), 0.12-0.08 (-$Si(CH_3)_3$).

1-2-4. Synthesis of homoarm star polymers

1-2-4-1. star-PMMA

Synthesis of PMMA star polymer (star-PMMA) was carried out by syringe technique under argon in baked glass flask equipped with a three-way stopcock. Precursor PMMA (14.9 g, M_n = 8,300, M_w/M_n = 1.25, 1.80 mmol), EGDMA (3.40 mL, 18.0 mmol), toluene (21.7 mL), and a solution of $Ru(Ind)Cl(PPh_3)_2$ in toluene (2.06 mM, 175 mL, 0.361 mmol), *n*-Bu_3N (0.858 mL, 3.61 mmol) were sequentially added into a 500 mL baked flask. Immediately after mixing, polymer solution was separated in three aliquots into the 100 mL flask at room temperature under argon. The mixtures were degassed by three freeze-pump-thaw cycles, and placed in an oil bath at 80 ºC. After 56 h, the reaction was terminated by cooling the mixtures in an ice bath. Solvent was removed under reduced pressure. The residue was dissolved in toluene (20wt%), and then the quintuple volume of methanol was poured into the polymer solution to

remove unreacted PMMA. The PMMA star was then dissolved in toluene and passed through silica gel and alumina columns to remove ruthenium complex. The solvent was concentrated under reduced pressure, and then polymer was precipitated with hexane. The precipitate was dried overnight under vacuum at room temperature to give final products as a white powder. M_w = 209,000, MWD =1.15 (SEC-MALLS). ^{1}H NMR (500.16 MHz, $CDCl_3$, $Si(CH_3)_4$ = 0 ppm): δ (ppm) = 3.70-3.40 (-OCH_3), 2.10-1.30 (-CH_2-), 1.30-0.60 (-CH_3).

1-2-4-2. star-PHEMA

A procedure similar to that described for star-PHEMA was applied to PTMSOEMA (10.8 g, 0.668 mmol, M_n = 16,200, M_w/M_n = 1.30), $Ru(Ind)Cl(PPh_3)_2$ (0.156 g, 0.134 mmol), toluene (67.5 mL), *n*-Bu_3N (0.32 mL, 1.34 mmol), EGDMA (1.26 mL, 6.68 mmol). The reaction time for the star polymer formation was 52h. The polymer was dissolved in acetone (20wt%), and then added into 4.9 times volume with water to remove unreacted PTMSOEMA. Ru-complex was removed by silica-gel and alumina column chromatographies eluted with toluene. TMS protecting group was removed by the addition of a small volume of 1.5 *N* HClaq. to the polymer solution in tetrahydrofuran. The resulting solution was poured into hexane to precipitate a star polymer. It was separated by suction filtration and dried under vacuum overnight at room temperature**:** M_w =286,000, MWD = 1.24 (SEC-MALLS), ^{1}H NMR (500.16 MHz, CD_3OD, $Si(CH_3)_4$ = 0 ppm): δ (ppm) = 4.17-3.91 (-CH_2-CH_2-OH), 3.89-3.66 (-CH_2-CH_2-OH), 2.20-1.44 (-CH_2-), 1.42-0.72 (-CH_3).

1-2-5. Synthesis of PHEMA / PMMA heteroarm star polymers

1-2-5-1. star-H47M53

All experimental procedures for synthesis of a series of heteroarm star polymers consisting of PHEMA and PMMA were similar to star PMMA synthesis. In a 100 mL round bottomed flask, PTMSOEMA (5.41 g, 0.334 mmol, M_n = 16,200, M_w/M_n = 1.30), PMMA (2.77 g, 0.334 mmol, M_n = 8,300, M_w/M_n = 1.25), Ru(Ind)Cl(PPh_3)$_2$ (0.156 g, 0.134 mmol), toluene (70.1 mL), *n*-Bu_3N (0.32 mL, 1.34 mmol), EGDMA (1.26 mL, 6.68 mmol) were added sequentially in this order at room temperature under argon. Immediately after the degassed by three freeze-pump-thaw cycles, the mixture was placed in an oil bath at 80 ºC. After 52 h, the reaction was terminated by cooling the mixture in an ice bath. The obtained star polymer was dissolved in toluene (20wt%), quintuple volume of methanol was added into the polymer solution to remove unreacted PMMA, and then the polymer was dried under reduced pressure. The polymer was dissolved in acetone (20wt%), and then added into 4.9 times volume with water to remove unreacted PTMSOEMA. Ru-complex was removed by silica-gel and alumina column chromatographies eluted with toluene. TMS protecting group was removed by the addition of a small volume of 1.5 *N* HClaq. to the polymer solution in ethanol/acetone (1/1 v/v). The resulting solution was poured into hexane to precipitate a star polymer. It was separated by suction filtration and dried under vacuum overnight at room temperature**:** M_w = 291,000, MWD = 1.39 (SEC-MALLS), HEMA/MMA = 46/54

(mol%). ^{1}H NMR (500.16 MHz, $CDCl_3/CD_3OD$ = 1/1, $Si(CH_3)_4$ = 0 ppm): δ (ppm) = 4.33-3.91 (-C*H*$_2$-CH$_2$-OH), 3.88-3.72 (-CH$_2$-C*H*$_2$-OH), 3.72-3.55 (-OC*H*$_3$), 2.31-1.40 (-C*H*$_2$-), 1.39-0.80 (-C*H*$_3$).

1-2-5-2. star-H71M29

A procedure similar to that described for star-H47M53 was applied to PTMSOEMA (8.13 g, 0.502 mmol, M_n = 16,200, M_w/M_n = 1.30), PMMA (1.39 g, 0.167 mmol, M_n = 8,300, M_w/M_n = 1.25), Ru(Ind)Cl(PPh$_3$)$_2$ (0.156 g, 0.134 mmol), toluene (68.8 mL), *n*-Bu$_3$N (0.32 mL, 1.34 mmol), EGDMA (1.26 mL, 6.68 mmol). The reaction time for the star polymer formation was 52h. M_w = 227,000, MWD = 1.17 (SEC-MALLS), PHEMA/PMMA = 71/29 (mol%). ^{1}H NMR (500.16 MHz, $CDCl_3/CD_3OD$ = 1/1, $Si(CH_3)_4$ = 0 ppm): δ (ppm) = 4.27-3.90 (-C*H*$_2$-CH$_2$-OH), 3.88-3.72 (-CH$_2$-C*H*$_2$-OH), 3.72-3.53 (-OC*H*$_3$), 2.31-1.40 (-C*H*$_2$-), 1.40-0.80 (-C*H*$_3$).

1-2-5-3. star-H22M78

A procedure similar to that described for star-H47M53 was applied to PTMSOEMA (2.71 g, 0.167 mmol, M_n = 16,200, M_w/M_n = 1.30), PMMA (4.16 g, 0.502 mmol, M_n = 8,300, M_w/M_n = 1.25), Ru(Ind)Cl(PPh$_3$)$_2$ (0.156 g, 0.134 mmol), toluene (71.4 mL), *n*-Bu$_3$N (0.32 mL, 1.34 mmol), EGDMA (1.26 mL, 6.68 mmol). The reaction time for the star polymer formation was 52 h. M_w =250,000, MWD =1.23 (SEC-MALLS), HEMA/MMA = 22/78 (mol%). ^{1}H NMR (500.16 MHz, $CDCl_3/CD_3OD$ = 1/1, $Si(CH_3)_4$ = 0 ppm): δ (ppm) = 4.33-3.95 (-C*H*$_2$-CH$_2$-OH), 3.91-3.74 (-CH$_2$-C*H*$_2$-OH), 3.74-3.54

(-OCH_3), 2.24-1.38 (-CH_2-), 1.38-0.80 (-CH_3).

1-2-6. lin-PHEMA 27k

A PHEMA with lower MW (lin-PHEMA 27k) was prepared by the deprotection of PTMSOEMA (precursor PTMSOEMA star). The TMS groups of the polymer were removed by HCl to give PHEMA from PTMSOEMA (M_w = 26,700): M_n = 20,000, MWD =1.34 (SEC). ^{1}H NMR (500.16 MHz, CD_3OD, Si(CH_3)$_4$ = 0 ppm): δ (ppm) = 4.18-3.91 (-CH_2-CH_2-OH), 3.91-3.67 (-CH_2-CH_2-OH), 2.20-1.44 (-CH_2-), 1.44-0.71 (-CH_3).

1-2-7. lin-PHEMA 290k

A PHEMA with higher MW (lin-PHEMA 290k) was prepared by free radical polymerization. AIBN (100 mg, 0.61 mmol), ethanol (22.6 mL), and HEMA (7.40 mL, 61 mmol) were added into a 100mL flask equipped with a three-way stopcock. After purged by argon bubbling for 15 min, the solution mixture was placed in an oil bath at 65 ºC for 2 h. The polymer was precipitated into acetone and collected by centrifugation. The precipitate was dried overnight under vacuum at room temperature: M_n = 162,000, M_w = 286,000, MWD = 1.77 (SEC). ^{1}H NMR (500.16 MHz, CD_3OD, Si(CH_3)$_4$ = 0 ppm): δ (ppm) = 4.18-3.91 (-CH_2-CH_2-OH), 3.91-3.67 (-CH_2-CH_2-OH), 2.20-1.44 (-CH_2-), 1.44-0.71 (-CH_3).

1-2-8. PHEMA/PMMA diblock copolymer (lin-Block)

PHEMA/PMMA diblock copolymer was synthesized under argon by the similar procedure described for synthesis of precursor PMMA. $Ru(Ind)Cl(PPh_3)_2$ (15.5 mg, 0.0180 mmol), toluene (3.41 mL), *n*-Bu_3N (0.159 mL, 0.180 mmol), TMSOEMA (3.92 mL, 18.0 mmol), and PMMA macroinitiator (M_n = 8,300, M_w = 10,400, MWD = 1.25, 1.49 g, 0.18 mmol) were added in a baked glass tube. The mixtures were placed in an oil bath at 80 ºC for 19 h. The diblock copolymer was precipitated into hexane, The Ru-complex was removed by silica-gel and alumina column chromatography eluted with toluene, and the TMS groups of polymer were removed by HCl. M_n = 26,300, M_w = 32,500, MWD = 1.23 (SEC). HEMA/MMA = 51/49 (mol%). ^{1}H NMR (500.16 MHz, $CD_3OD/CDCl_3$ = 1/1, $Si(CH_3)_4$ = 0 ppm): δ (ppm) = 4.21-3.94 (-C*H*$_2$-CH_2-OH), 3.80-3.40 (-CH_2-C*H*$_2$-OH), 3.50-3.40 (-OC*H*$_3$), 2.16-1.36 (-C*H*$_2$-), 1.36-0.70 (-C*H*$_3$).

1-2-9. HEMA/MMA random copolymer (lin-Random)

PHEMA/PMMA random copolymer was prepared by the same procedure described for polymerization of precursor PMMA. The monomers MMA and TMSOEMA were mixed in the polymerization to give a random copolymer. M_n = 24,500, M_w = 29,200, MWD = 1.19 (SEC), HEMA/MMA = 51/49 (mol%). ^{1}H NMR (500.16 MHz, $CD_3OD/CDCl_3$ = 1/1, $Si(CH_3)_4$ = 0 ppm): δ (ppm) = 4.21-3.94 (-C*H*$_2$-CH_2-OH), 3.80-3.40 (-CH_2-C*H*$_2$-OH), 3.50-3.40 (-O-C*H*$_3$), 2.16-1.36 (-C*H*$_2$-),

1.36-0.70 (-CH_3).

1-3. Calculation of number of arms

1-3-1. Determination of the ratio of arms in a star polymer

The HEMA and MMA monomer ratio of star polymers was determined by comparing the integrated intensities of the ^{1}H NMR signals from the side chain's ethylene group of HEMA (4.28-3.74 ppm) relative to the methyl of MMA (3.74-3.56 ppm). The PHEMA and PMMA ratio of star polymers was determined by the following relationship:

$$\frac{\text{HEMA ratio}}{\text{DP}_n \text{ of PHEMA}} : \frac{\text{MMA ratio}}{\text{DP}_n \text{ of PMMA}} = \text{PHEMA} : \text{PMMA}$$

1-3-2. Determination of the number of arms in star polymers

The numbers of arms in star polymers were determined based on ^{1}H NMR, SEC and SEC-MALLS analyses of precursor polymers and star polymers.

(a) star-PHEMA

The number of PHEMA arms in star-PHEMA, *f*(star-PHEMA), was estimated by molecular weights of star-PTMSOEMA and lin-PTMSOEMA. I assumed that

cross-linkers quantitatively reacted with precursor polymers to give star-PTMSOEMA, and the protecting groups (TMS) were also removed quantitatively.

$$f(\text{star-PHEMA}) = f(\text{star-PTMSOEMA}) = \frac{[M_w(\text{star-PTMSOEMA}) \times \text{WF(PTMSOEMA)}]}{M_w(\text{lin-PTMSOEMA})}$$

where f(star-PTMSOEMA), M_w(star-PTMSOEMA), WF(PTMSOEMA), M_w(lin-PTMSOEMA) represent the number of arms in star-PTMSOEMA, weight averaged molecular weight of star-PTMSOEMA measured by SEC-MALLS, weight fraction of PTMSOEMA arms in star-PTMSOEMA, and weight averaged molecular weight of lin-PTMSOEMA (M_w = 21,400) measured by SEC, respectively. The weight fraction of PTMSOEMA was calculated as follows:

$$\text{WF(PTMSOEMA)} = \frac{\text{W(PTMSOEMA)} \times \text{yield of star-PTMSOEMA}}{[\text{W(PTMSOEMA)} \times \text{yield of star-PTMSOEMA} + \text{W(EGDMA)}]}$$

where W(PTMSOEMA) and W(EGDMA) mean the weights of PTMSOEMA and EGDMA in the reaction solution. All the information was summarized in Table 1.

(b) star-PMMA

The number of PMMA arms in star-PMMA, f(star-PMMA), was estimated by molecular weights of star-PMMA and lin-PMMA. I assumed that cross-linkers quantitatively reacted with precursor polymers to give star-PMMA.

$$f(\text{star-PMMA}) = \frac{M_w(\text{star-PMMA}) \times \text{WF(PMMA)}}{M_w(\text{lin-PMMA 10k})}$$ where

f(star-PMMA), M_w(star-PMMA), WF(PMMA), M_w(lin-PMMA) represent the number of arms in star-PMMA, weight averaged molecular weight of star-PMMA measured by SEC-MALLS, weight fraction of PMMA arms in star-PMMA, and weight averaged molecular weight of lin-PMMA (M_w = 10,400) measured by SEC, respectively. The weight fraction of PMMA was calculated as follows:

$$\text{WF(PMMA)} = \frac{\text{W(PMMA)} \times \text{yield of star-PMMA}}{[\text{W(PMMA)} \times \text{yield of star-PMMA} + \text{W(EGDMA)}]}$$

where W(PMMA) and W(EGDMA) mean the weights of PMMA and EGDMA in the reaction solution. All the information was summarized in Table 1.

(c) Heteroarm star polymers

The number of arms in heteroarm star polymers, f(H$\underline{\text{X}}$M$\underline{\text{Y}}$), should be determined by the flowing equation:

$$f(\text{star-H}\underline{\text{X}}\text{M}\underline{\text{Y}}) = f(\text{star-PHEMA}) + f(\text{star-PMMA})$$

$$= \frac{M_w(\text{star-H}\underline{\text{X}}\text{M}\underline{\text{Y}}) \times \text{WF(PHEMA)}}{M_w(\text{lin-PHEMA 27k})} + \frac{M_w(\text{star-H}\underline{\text{X}}\text{M}\underline{\text{Y}}) \times \text{WF(PMMA)}}{M_w(\text{lin-PMMA 10k})}$$

where *f*(PHEMA), *f*(PMMA), WF(PHEMA), WF(PMMA), M_w(lin-PHEMA 27k), and M_w(lin-PMMA 10k) represent the number of arms of PHEMA and PMMA in the heteroarm star polymer, weight fraction of PHEMA and PMMA, weight averaged molecular weight of PHEMA and PMMA, respectively. (M_w(PHEMA) = 26,700, M_w(PMMA) = 10,400). However, it is difficult to determine of M_w(PHEMA) by means of SEC because the exclusion volume of PHEMA chain was much larger than that of PMMA chain having the same molecular weight. I thus estimated *f*(PHEMA) by the following equation:

$$f(\text{PHEMA}) = f(\text{PMMA}) \times \frac{r(\text{PHEMA})}{r(\text{PMMA})}$$

where *r*(PHEMA) and *r*(PMMA) represent the ratio of PHEMA and PMMA arms in the heteroarm star polymer *(NOT the ratio of monomers)*. They can be calculated the ratio of each monomer in ^{1}H NMR spectra and degree of polymerization of each polymer. *f*(H$\underline{\text{X}}$M$\underline{\text{Y}}$) can be thus determined by the following equation:

$$f(\text{star-H}\underline{\text{X}}\text{M}\underline{\text{Y}}) = f(\text{star-PHEMA}) \times \frac{r(\text{PHEMA})}{r(\text{PMMA})} + f(\text{PMMA})$$

All the information was summarized in Table 2.

1-4. Results and Discussion

1-4-1. Living radical polymerization of PTMSOEMA and PMMA

TMSOEMA and MMA were polymerized with small scale for determining of polymerization behavior by analysis of sampling solution. TMSOEMA or MMA was polymerized with the Ru catalyst and *n*-Bu_3N in toluene at 80 °C. The conversions smoothly reached over 90% in 24 h. As shown in Figure 1-2 and 1-5, the logarithmic conversion data, $\ln([M]_0/[M])$ ([M] is the monomer concentration at the time *t*), plotted against the time *t*, gave straight line passing, which shows constant concentrations of growing species during the polymerization. The number-average molecular weights (M_n) increased in direct proportion to monomer conversion and agreed with the calculated values based on the assumption that one molecule of the initiators generates one living polymer chain. The living radical polymerization of TMSOEMA or MMA can be achieved with the ECPA or MCPA/Ru(Ind)Cl$(PPh_3)_2$/*n*-Bu_3N to form polymers with controlled molecular weight and narrow $M_w/M_n < 1.3$ (Figure 1-3, 1-6). The purified polymers show the characteristic spectra of PMMA and PTMSOEMA . The terminal groups of the PMMA was analyzed by ^{1}H NMR after purification. As seen in Figure 1-4, the PMMA, the spectrum showed signals characteristic of the methine proton (*c*) of ester ethyl group at the α-end, along with the large absorptions of the main-chain PMMA units (e.g., *f* for the ester methyl). The number-average degrees of polymerization (DP_n) obteined from the peak intensity ratios *f*/*c* were 83 [DP_n(NMR, α-end)]. This was in close agreement with that by SEC [DP_n(SEC) = 81] calibrated

against standard PMMA. The terminal groups of the PTMSOEMA was similarly analyzed by ^{1}H NMR after purification. As seen in Figure 1-7, the PTMSOEMA, the spectrum showed signals characteristic of the methine proton (*b*) of ester methyl group at the α-end, along with the large absorptions of the main-chain PTMSOEMA units (e.g., *e* and *f* for the ethylene group). The number-average degrees of polymerization (DP_n) obteined from the peak intensity ratios *f*/*c* were 79 [DP_n(NMR, α-end)]. This was interestingly in close agreement with that by SEC [DP_n(SEC) = 79] calibrated against standard PMMA. This result indicated that PTMSOEMA and PMMA has similar excluded volume.

1-4-2. Polymer design and syntheses

A series of star polymers with different ratios of PHEMA and PMMA was prepared by the arm-mixing method. I first prepared linear PTMSOEMA (M_w =21,400, M_w/M_n = 1.31, DP_n = 79) and PMMA (M_w = 10,400, M_w/M_n = 1.25, DP_n = 81) as precursor polymers with almost same lengths for arms of star polymers by living radical polymerization using a Ru catalyst (Scheme 1). The hydroxy group of HEMA was protected by a TMS group prior to the polymerization, which facilitates the polymer preparation in non-polar organic solvents and avoids undesired interactions with the Ru catalyst during polymerization. The growing end groups of these precursor polymers were crosslinked by EGDMA using a Ru catalyst, giving a core-shell star shape structure. A SEC curve showed the formation of star-polymers as a new peak appeared at a higher molecular weight (MW) region (MW ~ 10^5) and only a trace

amount of precursor polymers (MW ~ 10^4) was observed (Figure 1-8, 1-10, 1-11,). The molecular weight distributions of the resultant star-polymers were relatively narrow (M_w/M_n = 1.15 – 1.39). These results suggest that the star polymers were prepared in a controlled and quantitative manner. The crude star polymers contained ca. 22 μmol/g-polymer of the residual Ru, as determined by MIP-MS. The purification of polymers by column chromatography using both silica gel and alumina columns significantly reduced the amount of the residual Ru to ca. 0.53 μmol/g-polymer.

The TMS protecting groups of PTMSOEMA were quantitatively removed by HCl treatment to give deprotected star polymers with PHEMA, as the peak at 0.2 ppm (TMS group) completely disappeared in the ^{1}H NMR spectrum (Figure 1-9, 1-10). The number of arms was 18-20 for all star-polymers except star-H71M29, which had 14 arms (Table 1, 2). The PHEMA star polymer and PMMA star polymers are referred to as star-PHEMA and star-PMMA, respectively. The heteroarm star polymers are denoted as star-H<u>X</u>M<u>Y</u> where X and Y indicate the mole percentage of PHEMA and PMMA arms, respectively. The arm ratios of PHEMA to PMMA arms of star polymers were determined by ^{1}H NMR analysis of purified heteroarm star polymers. I also prepared linear homopolymers lin-PHEMA 27k (M_w = 26,700) and 290k **(**M_w = 286,000) as well as an amphiphilic diblock copolymer lin-Block (51/49 mol%, M_w = 32,000) and random copolymer lin-Random (51/49 mol%, M_w = 29,200) for comparison.

1-4-3. Surface characterizations of coated surfaces

To test my strategy to prepare anti-fouling polymer coatings, I chose poly(ethylene terephthalate) (PET) as a model substrate of biomedical polymer materials in this study. PET has been widely used as a biomedical material for implants and artificial organs including artificial blood vessels [14] and heart valves [15]. PET films were coated by drop-casting of a polymer solution in organic solvents onto the PET film surface (Figure. 1-13). I used methanol for star-PHEMA or a mixture of methanol/acetone (1/1 v/v) for PHEMA/PMMA hetero-arm star polymers because of the low solubility of PMMA arms with methanol. The coating solvent was first evaporated at room temperature, and then the coatings were dried under reduced pressure overnight.

The surface morphology and topographical structures are key determinants for anti-adhesion properties of polymer coatings against proteins, cells, and bacteria [16-18]. I first examined the polymer-coated surfaces by SEM (Figure 1-14). The PET surface coated by lin-PHEMA 27k was relatively smooth. Interestingly, star-PHEMA formed fibrous aggregates, resulting in a network structure covering the entire substrate surface, which is likely reflected by the translucency of coated film. The difference in the surface structures between the linear and star polymers indicates that the star-polymer architecture of star-PHEMA is responsible for the formation of aggregates possibly due to the high density of polymer chains, enhancing the polymer packing and entanglement. It has been previously reported that star-shaped poly(L-lactic acid) polymers

self-assembled to nanofibrous structures forming hollow microspheres [19]. In contrast, the coating of star-H71M29 showed relatively rough surfaces, but no distinctive topographical structure was observed, giving the transparent films. The star-PMMA showed clustering of small aggregates with a relatively uniform size, forming an island-sea structure on the surface. The reasons for the heteroarm star polymer-coated surfaces make relatively flat surface and non-aggregated layer might be explaimed as follows. Either the PMMA chains may aggregate into a molecule core of heteroarm star polymer in MeOH/aceton (1/1= v/v) or aggregated PHEMA chains and PMMA chains form a phase-separated structure. These phenomenon resulted in the inhibition of auto-aggregation at coating and increased the stability of the coated layer. In the future, more detailed discussion should be made based on analysis of heteroarm star polymers such as glass-transition temperature.

On the other hand, a number of small aggregates were scattered on the coating of lin-PMMA 10k (Figure 1-14). These results indicate that the surface structure of coatings depends on the polymer structures (star vs. linear) as well as the properties (PHEMA vs. PMMA). The homo-star polymers (PHEMA and PMMA star polymers) tend to form aggregate structures on the surface, likely due to the high density of polymer chains. However, the heteroarm star polymers containing both PMMA and PHEMA polymer chains render the coatings more homogeneous, suggesting the polymer aggregation and surface morphology can be controlled by the polymer arm composition of star polymers.

The microscopic structures of polymer coatings were examined by AFM. The PET surface and polymer coatings displayed some roughness, giving

root-mean square (RMS) roughness of 4.69 (PET), 0.428 (lin-PHEMA 27k), 60.3 (star-PHEMA), 36.5 (star-H71M29) and 328 nm (star-PMMA). Interestingly, all surfaces coated by the star polymers had spherical structures 36-78 nm in diameter and 2.6-17 nm in height, while the linear polymer PHEMA 27k did not show any specific surface structures (Figure 1-15). These results attribute the spherical structure consisted of individual star polymer or possibly aggregates of multiple star polymers. To that end, the size of star polymers in the 0.1 wt% casting solvents (star-PHEMA: methanol, star-H71M29 - star-H22M78 : methanol/acetone = 1/1 v/v, star-PMMA: acetone) were determined by dynamic light scattering (DLS). The values of hydrodynamic radius of star polymers in the coating solvents were 19.0 (star-PHEMA), 17.3 (star-H71M29), 39.3(star-H47M53), 17.2 (star-H22M78) and 14.8 nm (star-PMMA), with a relatively narrow distribution. This suggests that the multiple star polymers form spherical aggregates on the coatings, likely during the casting and drying processes because of it was not allowed in coating solvents from DLS data. It is difficult to directly measure the density of PHEMA arms on the star polymer-coated surfaces.

The density of PHEAM arms was estimated as follows. If the size of adsorbed star-H71M29 is the same with the size of star-H71M29 solved in MeOH/aceton (1/1 v/v) (Figure 1-16), the projection area (= πr^2) of star-H71M29 particle is calculated to be 235 nm^2 from diameter (17.3 nm) of star-H71M29 in the solution by DLS. The number of PHEMA arms of the star-H71M29 is calculated to be 12 based on the result of GPC-MALLS in DMF. If all the PHEMA arms are enough dispersed on the 235 nm^2, the PHEMA arm density of star-H71M29-coated surface is 0.05 arms/nm^2. The

density is similar to that of PHEMA brush described in literature [25]. Therefore, star-H71M29-coated surface is assumed to have similar graft-like structure and functionality of the PHEMA brush surface.

1-4-4. Wettability of polymer coatings

To determine the wettability of the coated surfaces, I measured the static contact angles of water droplets and air-bubbles on the polymer coating (Figure 1-17). Wettability of surfaces plays an important role in the adhesion mechanisms of proteins and cells. In general, hydrophilic surfaces reduce the non-specific hydrophobic adhesion of proteins and cells, which is the initial key step in the bio-fouling mechanism. However, the wettability of surfaces does not directly relate to their ability to inhibit adhesion of biomolecules and cells, and it is known that the anti-adhesion activity of surfaces is also affected by polymer architectures [20], freezing bound water on surfaces [21], and the functionality of surface groups [22]. The contact angle of non-coated PET was 65° by the sessile drop method. The contact angles of 39° for star-PHEMA and 43° for lin-PHEMA 290k are similar, although their polymer structures (star vs. linear) and surface morphologies (network vs. smooth surface) are significantly different. The contact angle increased as the PMMA ratio of star polymers increased from 52% to 71% (Table 1). This indicates that the hydrophobic PMMA increased the hydrophobicity of coating surfaces.

The static water contact angles determined above reflect the wettability of dry

surfaces [23]. However, adhesion of proteins and bacteria generally occurs in aqueous environment, and the surface property in water is likely more related to the anti-adhesion activity of coatings. To that end, I determined the contact angle of air-bubbles adherent on the coatings incubated in water at 37 °C for 12 h. The contact angles of lin-PHEMA 27k and 290k coatings were 153º and 159º, respectively. Unfortunately, contact angels of the star-PHEMA and heteroarm star polymers could not be measured because air bubbles were not adsorbed on the coating surfaces, indicating these coatings are highly hydrophilic. This suggests that hydrophilic PHEMA star polymer arms are hydrated and expanded into water during incubation, increasing the hydrophilicity and constituting high density polymer brush structures [24]. Compared to lin-PHEMA, expanded PHEMA arms of star polymers are hydrated with a larger number of water molecules, result in a large hydrated layer inhibiting air-bubble adsorption (Figure 1-18). The high hydrophilicity of the coatings reveals to reflect the anti-adhesion activity of coatings against platelets and bacteria (to be discussed further below). In this study, air-in-water (captive bubble drop) contact angle was not directly made a comparison between PHEMA brush surface and star polymer having PHEMA arms. Moreover, the air-in-water (captive bubble drop) contact angle of PHEMA brush surface has not yet been reported. However, PHEMA brush surface might possibly indicate that inhibition of air-bubble adsorption as well as star polymer-coated surface because star polymer surfaces having PHEMA arms provide the brush like structure.

1-4-5. Scratch test

To examine the physical durability of coatings, I evaluated scratch resistance of the polymer coatings by measuring the scratch width caused by different load (Figure 1-18A). The scratch width of the star-PHEMA coating was 40 μm at 4.9 mN load and increased to 50 μm as the loading strength was increased to 19.6 mN and 49 mN (Figure 1-18B) Conversely, the star-H71M29 displayed no scratch at 4.9 mN, and the scratch width was 22 μm at 19.6 mN, which was significantly smaller than that of the star-PHEMA coating. These results indicate that the star-H71M29 is not readily scratched compared to the star-PHEMA. In general, scratch resistance reflects the mechanical strength and adhesiveness of coatings to substrates. From this result, star-H71M29 provides a relatively homogeneous coating structure with higher mechanical strength and adhesiveness to a PET surface than the heterogeneous coating by the PHEMA star polymer. This may be due to the properties of PMMA, which display good adhesiveness to plastic materials and hardness in general. The mechanical durability of star-H71M29 coating will facilitate the handling of coated materials as well as usefulness for applications such as coating of catheters and devices where mechanical strength in a coating is desired.

To examine the micro-structures of coating layers in more detail, the marginal portion of the scratch was further examined by AFM. The star PHEMA coating has a homogeneous coating layer with a thickness of ~11 nm and aggregate structures with height of ~250 nm, which is likely to be a part of the macroscopic fibrous network

structure of coating observed in the SEM image (Figure 1-19). This indicates that the star-PHEMA coating consists of a three-dimensional network structure on the underlying homogeneous coating layer. It should be noted that non-coated PET surface did not show any scratch at 49 mN loading. Therefore, the bottom layer of star-PHEMA is not an artifact due to the scratched PET. On the other hand, the star-H71M29 coating had one layer with a thickness of ~140 nm, indicating that the heteroarm star polymer provide homogeneous coating surfaces. The heteroarm star polymer admits improving the stability with increasing hydrophobic chain ratio in star polymers.

1-5. Conclusions

The living radical polymerization of MMA and TMSOEMA proceeded successfully. Interestingly, the polymerization behaviors were similar with Ru catalyst in toluene.

Heteroarm and homoarm star polymers consisting of PHEMA and/or PMMA were synthesized by living radical polymerization with a Ru complexes as catalysts. Ru complex was almost removed by silica gel and alumina gel chromatography purification methods. By systematically changing the molar ratios of PHEMA and PMMA heteroarm star polymers with different arm compositions were obtained. The arm compositions in different PHEMA/PMMA heteroarm star polymers were in agreement with the molar ratios of PTMSOEMA/PMMA in initial mixture, respectively. The

polymer synthesis and coating preparation is facile compared to other methods for providing hydrophilic surfaces.

Heteroarm star polymer (star-H71M29) had similar wettability with star-PHEMA, but surface strength was clearly consolidated compared to star-PHEMA.

By introducing hydrophobic arms to star polymers, stability was increased with maintenance of wettability of the coating surface.

1-6. References

[1] Kamigaito M, Ando T, Sawamoto M. Metal-catalyzed living radical polymerization. Chem Rev 2001;101:3689-745.

[2] Kamigaito, M.; Ando, T.; Sawamoto, M. Metal-catalyzed living radical polymerization: discovery and developments. Chem Rec 2004;4:159-75.

[3] Ouchi M, Terashima T, Sawamoto M. Precision control of radical polymerization via transition metal catalysis: from domant species to designed catalysts for precision functional polymers. Acc Chem Res 2008, 41, 1120-32.

[4] Ouchi M, Terashima T, Sawamoto M. Transition metal-catalyzed living radical polymerization: toward perfection in catalysis and precision polymer synthesis. Chem Rev 2009;109:4963-5050.

[5] Gao H, Matyjaszewski K. Synthesis of functional polymers with controlled architecture by CRP of monomers in the presence of cross-linkers: from stars to gels. Prog polym sci 2009, 34, 317-50.

[6] Baek KY, Kamigaito M, Sawamoto M. Star-shaped polymers by metal-catalyzed living radical polymerization. 1. design of Ru(II)-based systems and divinyl linking agents. Macromolecules 2001, 34: 215-21.

[7] Beak KY, Kamigaito M, Sawamoto M. Star-shaped polymers by Ru(II)-catalyzed living radical polymerization. II. Effective reaction conditions and characterization by multi-angle laser scattering/size exclusion chromatography and small-angle X-ray scattering. J Polym Sci Part A Polym Chem 2002;40:2245-55.

[8] Terashima T, Ouchi M. Ando T, Kamigaito M, Sawamoto M. Amphiphilic, thermosensitive rutenium(II)-bearing star polymer ruthenium(II)-enclosed microgel cores via metal-catalyzed living radical polymerization. J polym Sci Part A: Polym Chem 2010;48:373-9.

[9] Terashima T, Ouchi M. Ando T, Kamigaito M, Sawamoto M. Amphiphilic, thermosensitive Ruthenium(II)-Bearing star polymer catalysts: one-pot synthesis of PEG armed star polymers with rutenium(II)-enclosed microgel cores via metal-catalyzed living radical polymerization. Macromolecules 2007;40:3581-88.

[10] Kusmaatmaja A, Ando T, Terada K, Hirohara S, Nakashima T, Kawai T, Terrashima T, Tanihara M. Synthesis and photoproperties of Eu(III)-bearing star polymers as luminescence materials. J polym Sci Part A: Polymer Chem 2013;51:2527-35.

[11] Baek KY, Kamigaito M, Sawamoto M. J Polym Sci Part A Polymer Chem 2002;40:633-41.

[12] Baek KY, Kamigaito M, Sawamoto M. Coer-Functionalized star polymers by transition metal-catalyzed living radical polymerization. 2. Selective interaction with protic guests via core functionalities. Macromolecules 2002;35: 1493-98.

[13] Hirao A, Kato H, Yamaguchi K, Nakahama S. Macromolecules 1986, Polymerization of monomers containing functional groups protected by trialkylsilyl groups. 5. synthesis of poly(2-hydroxyrthyl methacrylate) with a narrow molecular weight distribution by means of anionic living polymerization. 19,1294-99.

[14] Ramakrishna S, Mayer J, Wintermantel E, Leong KW. Biomadical applications of polymer-composite materials: A review. Compos Sci Technol 2001;61:1189-224.

[15] Tokunaga S, Tominaga R. Artificial valves "up to date" in Japan. J Artif Organs 2010;13:77-87.

[16] Mei L, Busscher HJ, Van der Mei HC, Ren Y. Influence of surface roughness on streptococcal adhesion forces to composite resins. Dent Mater 2011;27:770-8.

[17] Koh LB, Rodriguez I, Venkatraman SS. The effect of topography of polymer surfaces on platelet adhesion. Biomaterials 2010;31:1533-45.

[18] Palacio MLB, Schricker SR, Bhushan B. Bioadhesion of various proteins on random, diblock and triblock copolymer surfaces and the effect of pH conditions. J R Soc Interface 2011;8:630-40.

[19] Liu X, Jin X, Ma PX. Nanofibrous hollow microspheres self-assembled from star-shaped polymers as injectable cell carriers for knee repair. Nat Mater 2011;10:398-406.

[20] Nagaoka S, Nakao A. Clinical application of antithrombogenic hydrogel with long poly(ethylene oxide)chains. Biomaterials 1990;11:119-21.

[21] Tanaka M, Mochizuki A. Effect of water stracture on blood compatibility-thermal analysis of water in poly(meth)acrylate. J Biomed Mater Res 2004;68:684-95.

[22] Ostuni E, Chapman RG, Holmlin RE, Takayama S, Whitesides GM. A Survey of stracture-property relationships of surfaces that resist that the adsorption of protein. Langmuir 2001;17:5605-20.

[23] Tsukagoshi T, Kondo Y, Yoshino N. Protein adsorption on polymer-modified silica particle surface. Colloids Surf B 2007;54:101-7.

[24] Kitano H, Imai M, Mori T, Gemmei-Ide M, Yokoyama Y, Ishihara K. Structure of water in the vicinity of phospholipid analogue copolymers as studied by vibrational spectroscopy. Langmuir 2003;19:10260-6.

[25] Yoshikawa C, Goto A, Tsujii Y, Fukuda T, Kimura T, Yamamoto K, Kishida. Protein repellency of well-defined concentrated poly(2-hydroxyethyl methacrylate) brushes by size-exculusion effect. Macromolecules 2006;39:2284-90.

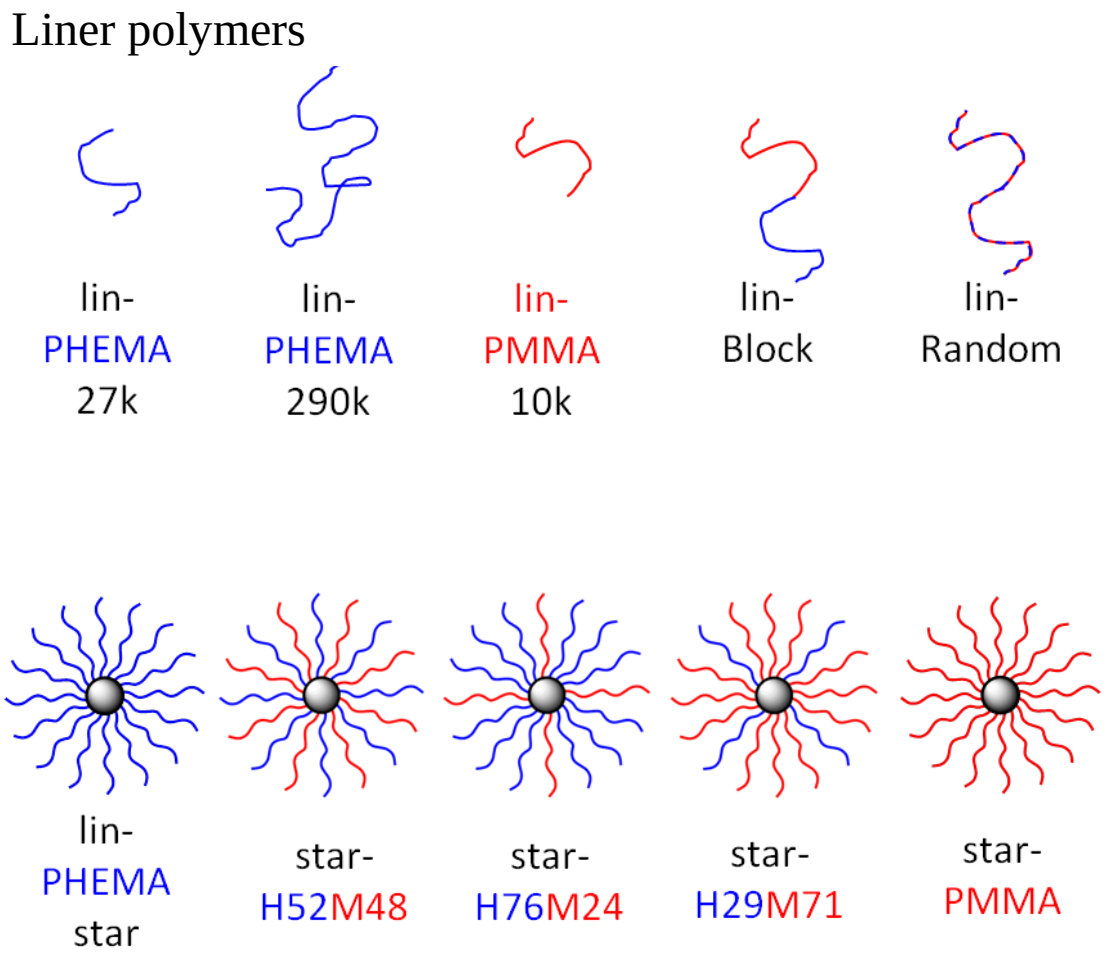

Figure 1-1. The structures of polymers used in this study.

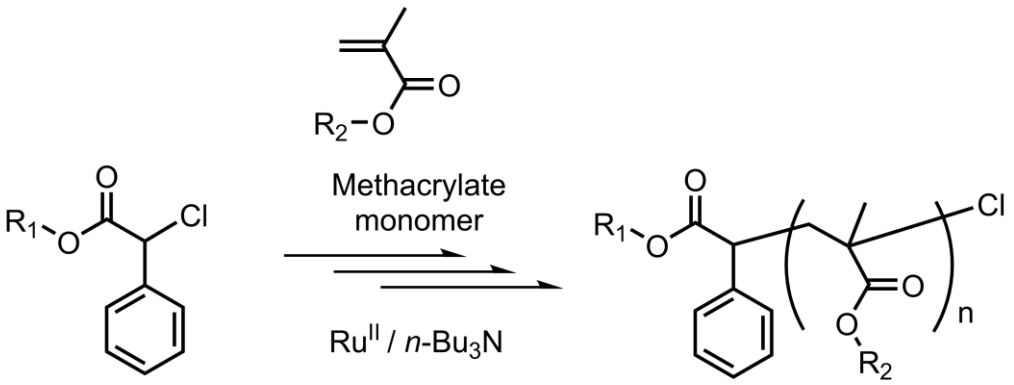

	Initiator (R_1)	**Methacrylate monomer (R_2)**	**Catalyst (Ru^{II})**
Precursor PHEMA arm	$-CH_3$ MCPA	$-CH_2CH_2-O-Si(CH_3)_3$ TMSOEMA	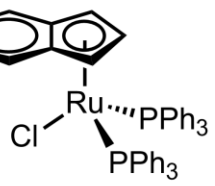
Precursor PMMA arm	$-CH_2CH_3$ ECPA	$-CH_3$ MMA	$Ru(Ind)Cl(PPh_3)_2$

Scheme 1-1. Polymerization of TMSOEMA and MMA

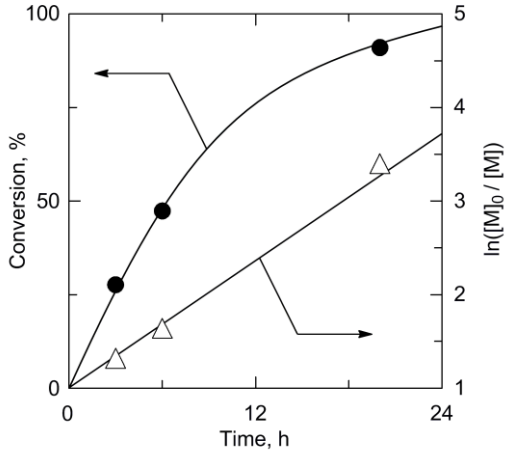

Figure 1-2. Time-conversion curves for the polymerization of MMA with ECPA/Ru(Ind)Cl(PPh_3)$_2$/*n*-Bu_3N in toluene at 80 °C: $[MMA]_0$ = 4000 mM; $[ECPA]_0$ = 40 mM; $[Ru(Ind)Cl(PPh_3)_2]_0$ = 4.0 mM; [*n*-$Bu_3N]_0$ = 40 mM.

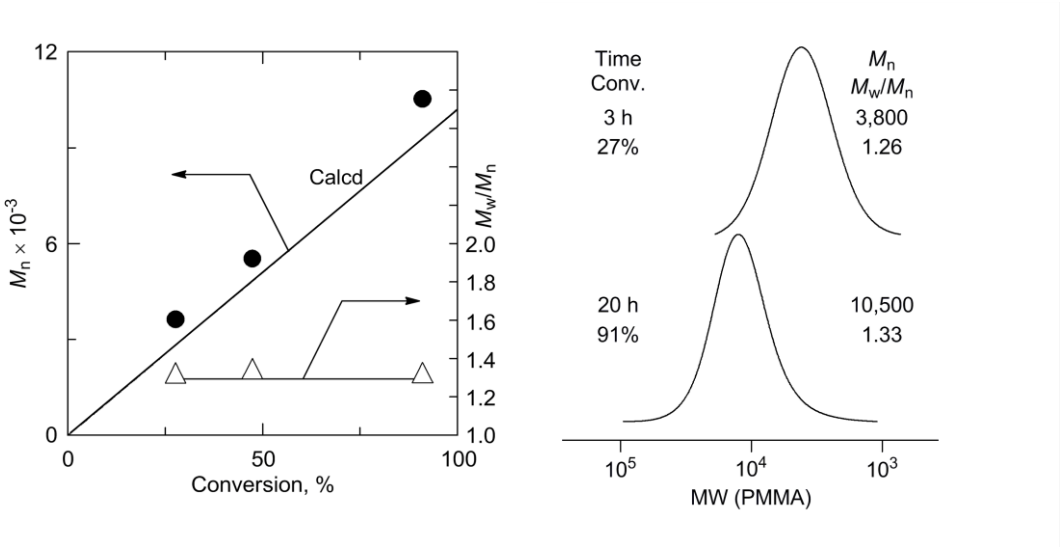

Figure 1-3. M_n, M_w/M_n, and MWD curves of PMMA obtained with ECPA/ $Ru(Ind)Cl(PPh_3)_2$/ *n*-Bu_3N in toluene at 80 ºC: $[MMA]_0 = 4000$ mM; $[ECPA]_0 = 40$ mM; $[Ru(Ind)Cl(PPh_3)_2]_0 = 4.0$ mM; $[n\text{-}Bu_3N]_0 = 40$ mM.

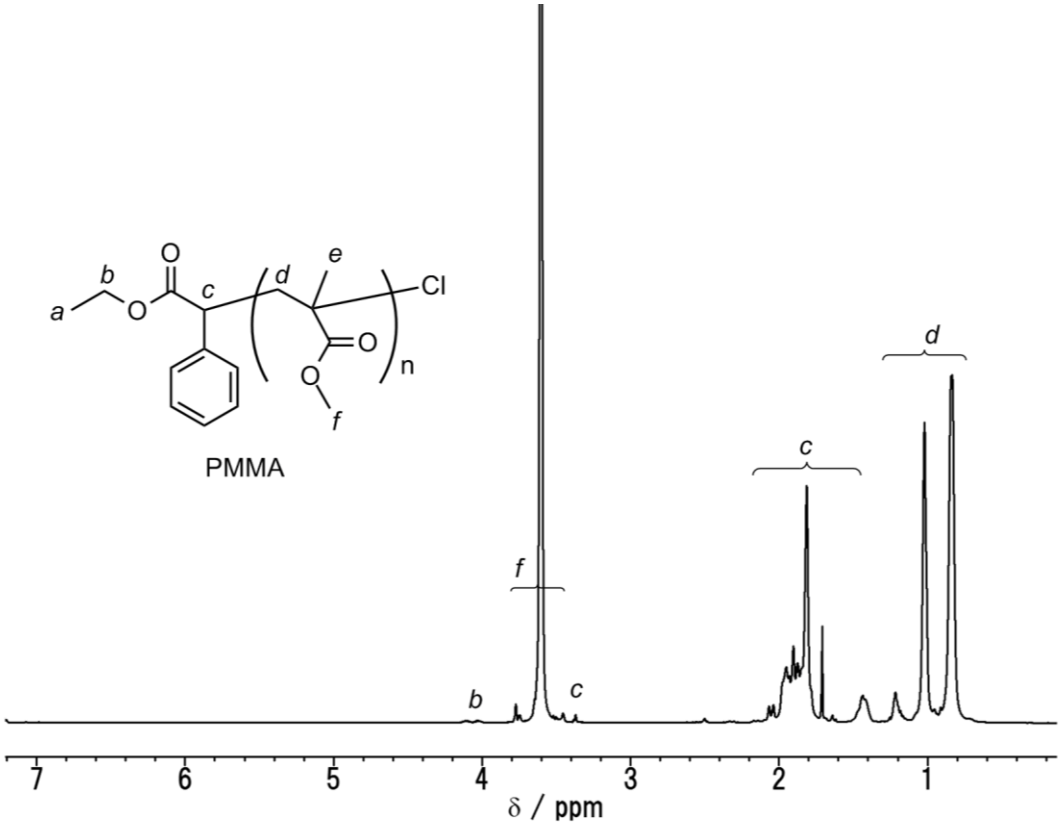

Figure 1-4. ^{1}H NMR spectrum of PMMA in $CDCl_3$ at room temperature.

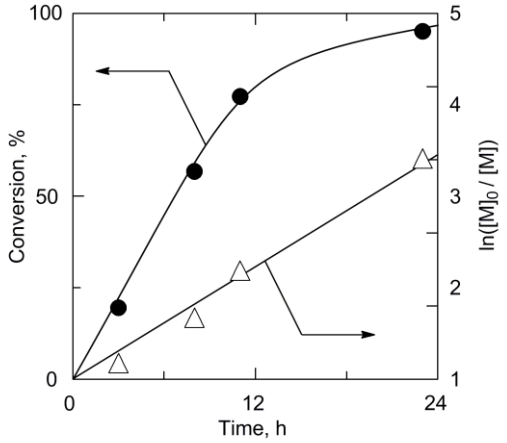

Figure 1-5. Time-conversion curves for the polymerization of TMSOEMA with ECPA/ $Ru(Ind)Cl(PPh_3)_2$/ *n*-Bu_3N in toluene at 80 °C: $[TMSOEMA]_0$ = 4000 mM; $[ECPA]_0$ = 40 mM; $[Ru(Ind)Cl(PPh_3)_2]_0$ = 4.0 mM; [*n*-$Bu_3N]_0$ = 40 mM.

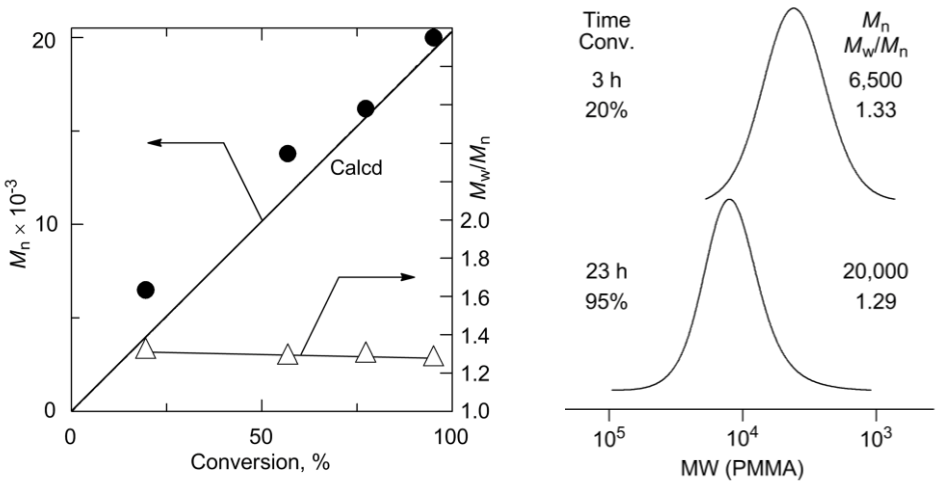

Figure 1-6. M_n, M_w/M_n, and MWD curves of PTMSOEMA obtained with ECPA/Ru(Ind)Cl(PPh_3)$_2$/*n*-Bu_3N in toluene at 80 ºC: $[MMA]_0$ = 4000 mM; $[ECPA]_0$ = 40 mM; $[Ru(Ind)Cl(PPh_3)_2]_0$ = 4.0 mM; [*n*-$Bu_3N]_0$ = 40 mM.

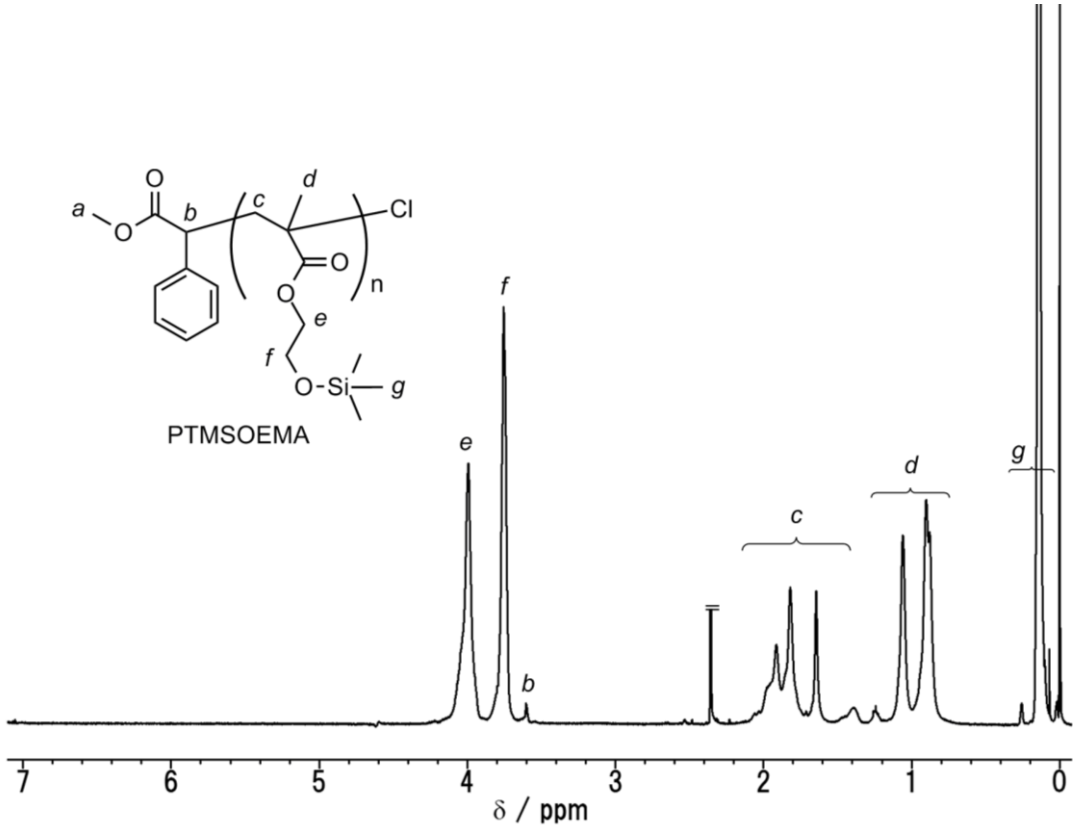

Figure 1-7. ^{1}H NMR spectrum (in $CDCl_3$ at room temperature) of PTMSOEMA.

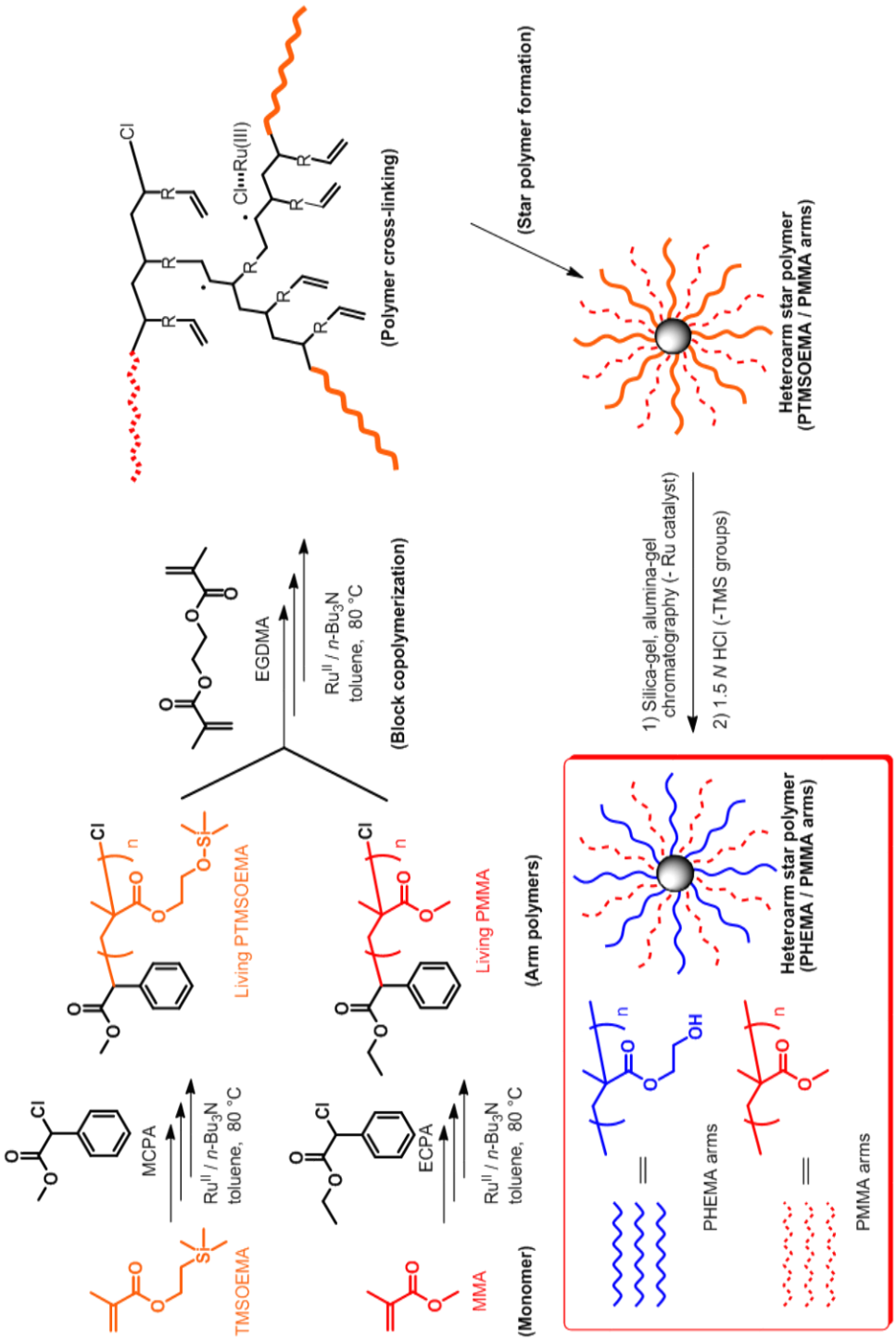

Scheme 1-2. Synthesis of PHEMA/PMMA homo- or heteroarm star polymer via Ru(II)-catalyzed living radical polymerization

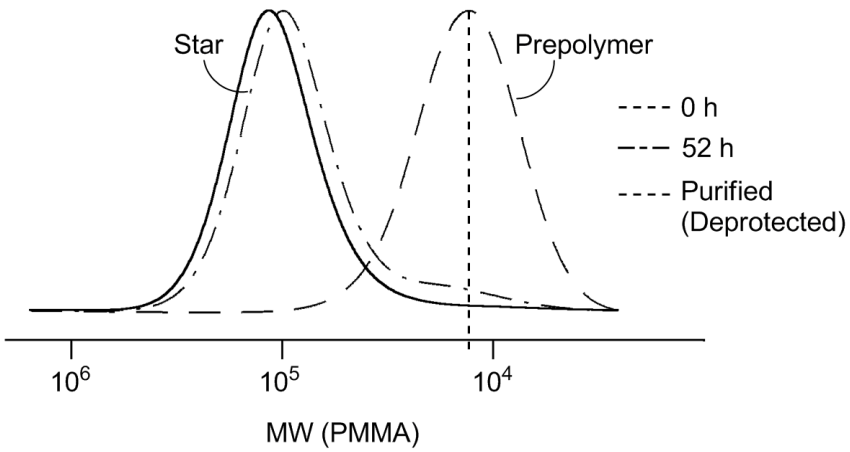

Figure 1-8. GPC curves of star-H52M48 during the synthesis by cross-linking of PTMEOEMA and PMMA with equal moles; experimental conditions: $[PTMSOEMA]_0$= 4.18 mM; $[PMMA]_0$= 4.18 mM; $[EGDMA]_0$= 83.5 mM; $[Ru(Ind)Cl(PPh_3)_2]_0$= 1.67 mM; $[n\text{-}Bu_3N]_0$= 16.7 mM, at 80 ºC in toluene.

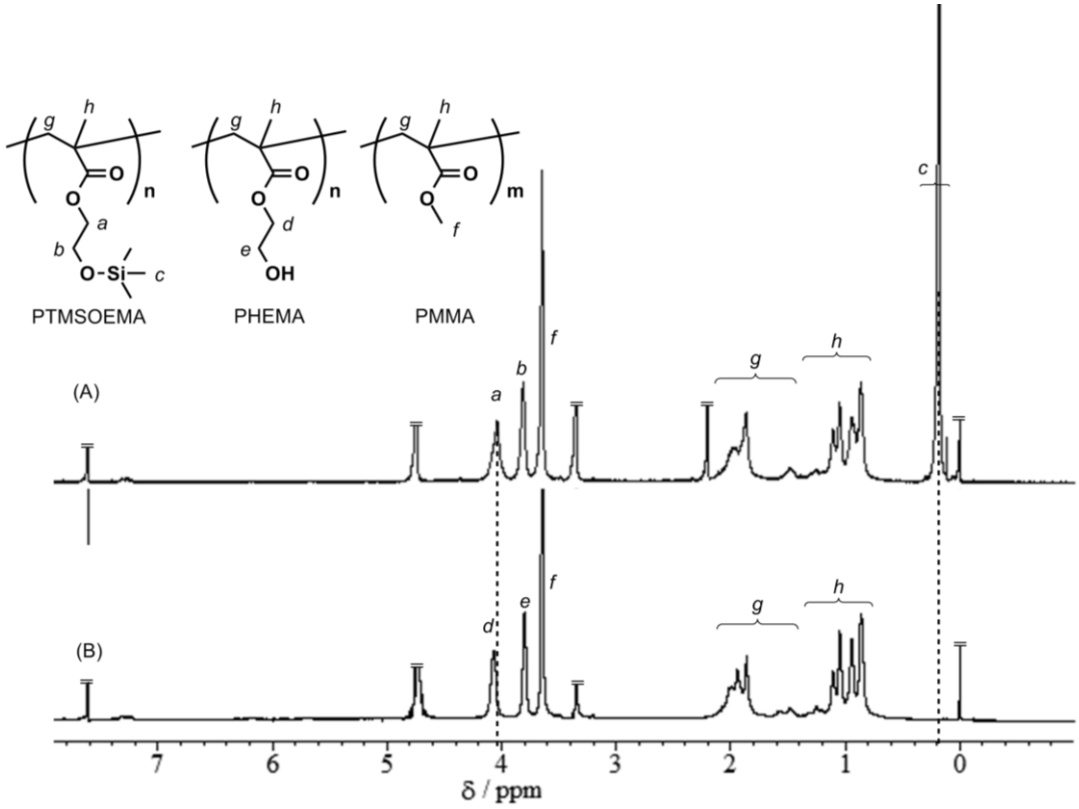

Figure 1-9. ^{1}H NMR spectra (in $CD_3OD/CDCl_3$ = 1/1 at room temperature) of star-H52M48 (A) before (PTMSOEMA arm/PMMA arm) and (B) after deprotection, 50/50 heteroarm star polymers (PHEMA arm/PMMA arm).

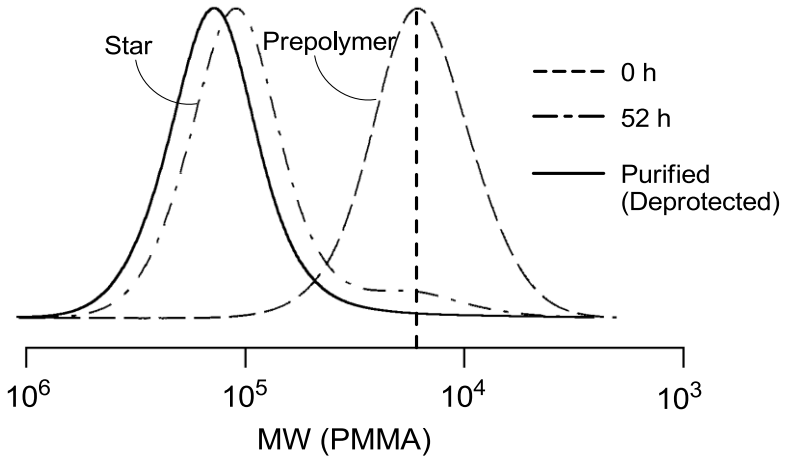

Figure 1-10. GPC curves of star-H71M29 during the synthesis by crosslinking of PTMEOEMA and PMMA with PTMSOEMA / PMMA (75/25 mol%) experimental conditions: $[PTMSOEMA]_0$= 6.27 mM; $[PMMA]_0$= 2.09 mM; $[EGDMA]_0$= 83.5 mM; $[Ru(Ind)Cl(PPh_3)_2]_0$= 1.67 mM; $[n\text{-}Bu_3N]_0$= 16.7 mM, at 80 ºC in toluene.

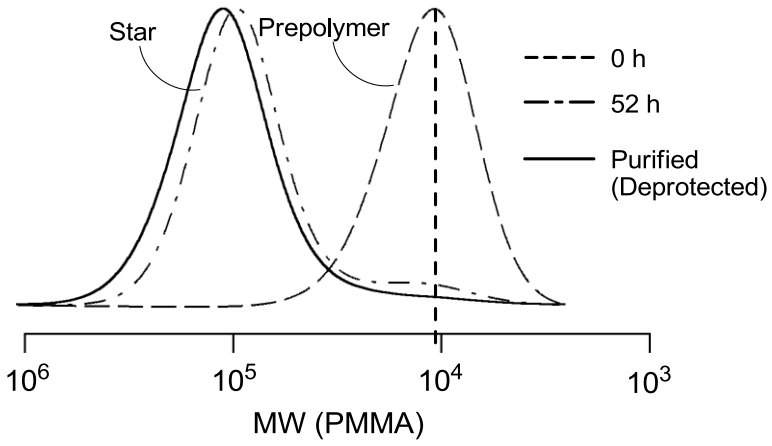

Figure 1-11. GPC curves of star-H29M71 during the synthesis by crosslinking of PTMEOEMA and PMMA PTMSOEMA / PMMA (25/75 mol%); experimental conditions: $[PTMSOEMA]_0$= 2.09 mM; $[PMMA]_0$= 6.27 mM; $[EGDMA]_0$= 83.5 mM; $[Ru(Ind)Cl(PPh_3)_2]_0$= 1.67 mM; $[n\text{-}Bu_3N]_0$= 16.7 mM, at 80 ºC in toluene.

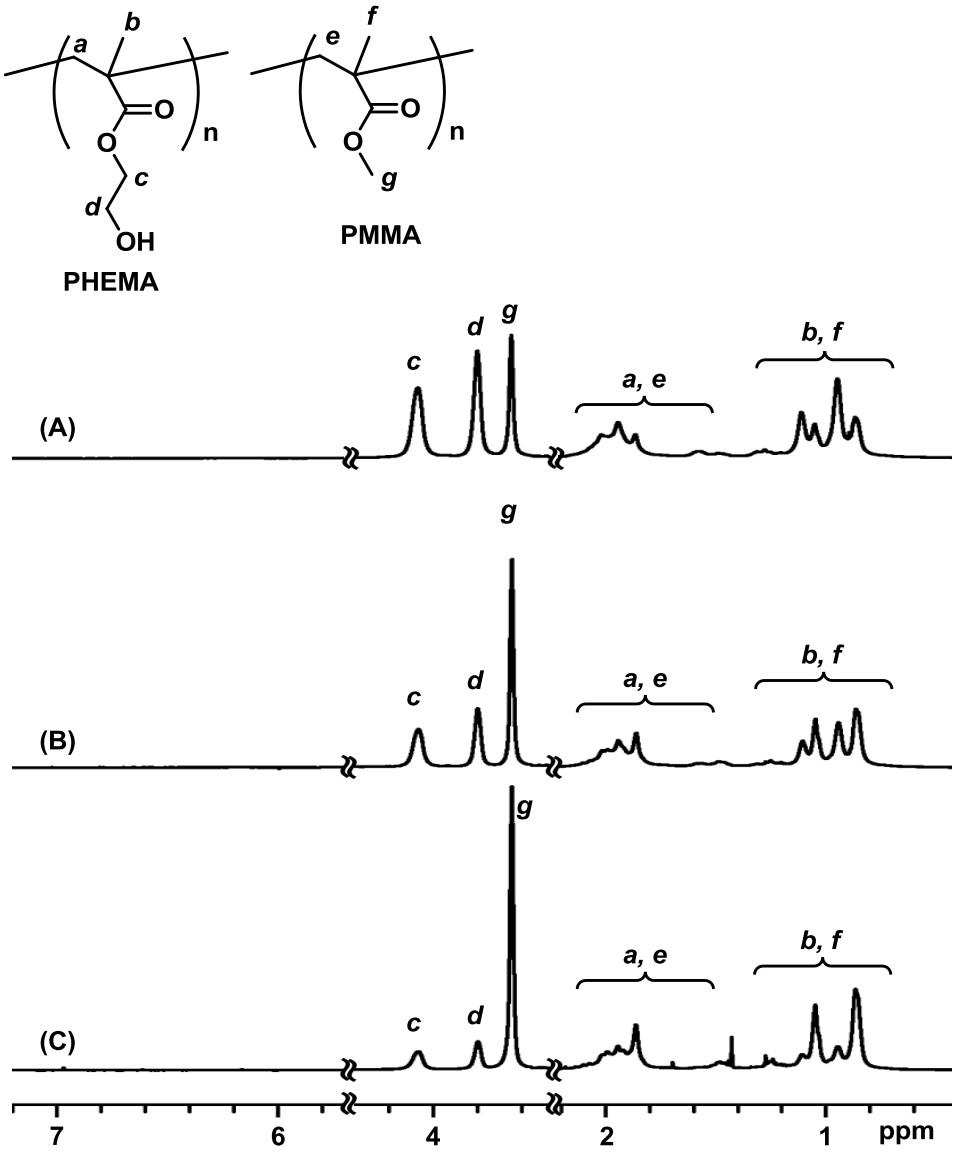

Figure 1-12. ^{1}H NMR spectra (in $CD_3OD/CDCl_3$ = 1/1 at room temperature) of (A) star-H71M29, (B) star-H48M52, (C) star-H29M71 (PHEMA arm/PMMA arm).

Table 1. Characterization of linear and star polymers.

lin-PHEMA 27k	Linear	26,700a)	1.34c)	1.00/0.00	1 (1:0)	21±4.2	153±10
lin-PHEMA 290k	Linear	286,000a)	1.77c)	1.00/0.00	1 (1:0)	43±1.7	159±5.1
star-PHEMA	Star	286,000b)	1.24d)	1.00/0.00	20 (20:0)	39±0.6	-i)
star-H71M29	Star	227,000b)	1.17d)	0.71/0.29	14 (10:4)	45±2.6	-i)
star-H47M53	Star	291,000b)	1.39d)	0.47/0.53	19 (9:10)	47±1.5	-i)
star-H22M48	Star	250,000b)	1.23d)	0.22/0.78	18 (4:14)	53±3.6	-i)
star-PMMA	Star	209,000b)	1.15d)	0.00/1.00	16 (0:16)	73±1.8	137±10
lin-PMMA 10k	Linear	10,400a)	1.25c)	0.00/1.00	1 (0:1)	71±2.4	125±2.4
lin-Block	Linear	32,500a)	1.23c)	-f)	2 (1:1)	43±5.1	155±11
lin-Random	Linear	29,200a)	1.19c)	-f)	1	45±3.4	126±4.8

a) The weight-average molecular weight (M_w) was determined by SEC. b) determined by SEC-MALLS. c) M_w/M_n was determined by SEC. d) determined by SEC-MALLS. e) The molar ratios of PHEMA to PMMA units of star polymers. See Supporting Information for calculation. f) The HEMA and MMA monomer units of lin-Block and lin Random were 0.52/0.48, 0.51/0.49). g) The total number of arms in a star polymer. The numbers of PHEMA and PMMA arms were given in parentheses. See Supporting Information for calculation. h) Contact angles of the water droplets (sessile drop) and air-in-water (captive bubble drop). i) not determined due to no adhesion of air bubbles.

Table 2. The number of PHEMA and PMMA arms in heteroarm star polymers.

Star polymers	M_w (star-H<u>X</u>M<u>Y</u>)[a]	WF (PMMA)	*r* (PHEMA)	*r* (PMMA)	Yield of star (%)	Monomer mole ratio (HEMA:MMA) [a]	Polymer mole ratio (PHEMA:PMMA)	Total number of arms, *f*(H<u>X</u>M<u>Y</u>)	PHEMA arms, *f*(PHEMA)	PMMA arms, *f*(PMMA)
star-H71M29	227,000	0.17	0.71	0.29	95	0.70:0.30	0.71:0.29	14	10	4
star-H47M53	291,000	0.36	0.47	0.53	93	0.46:0.54	0.47:0.53	19	9	10
star-H22M78	250,000	0.57	0.22	0.78	96	0.22:0.78	0.22:0.78	18	4	14

a) determined by ^{1}H NMR analysis of depotected star-polymers.

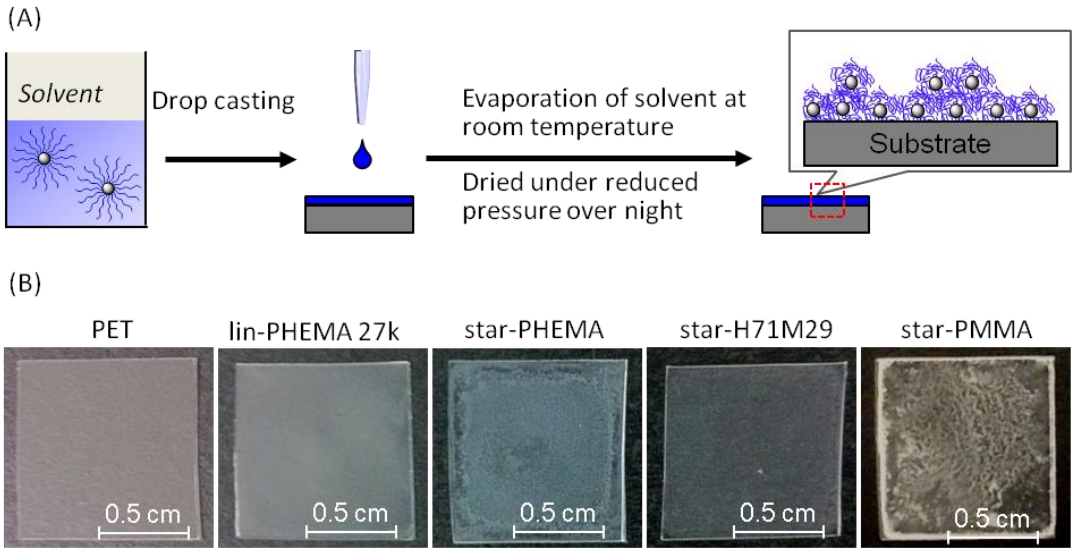

Figure 1-13. Drop cast methods of polymer solutions and photographs of polymer coated surfaces.

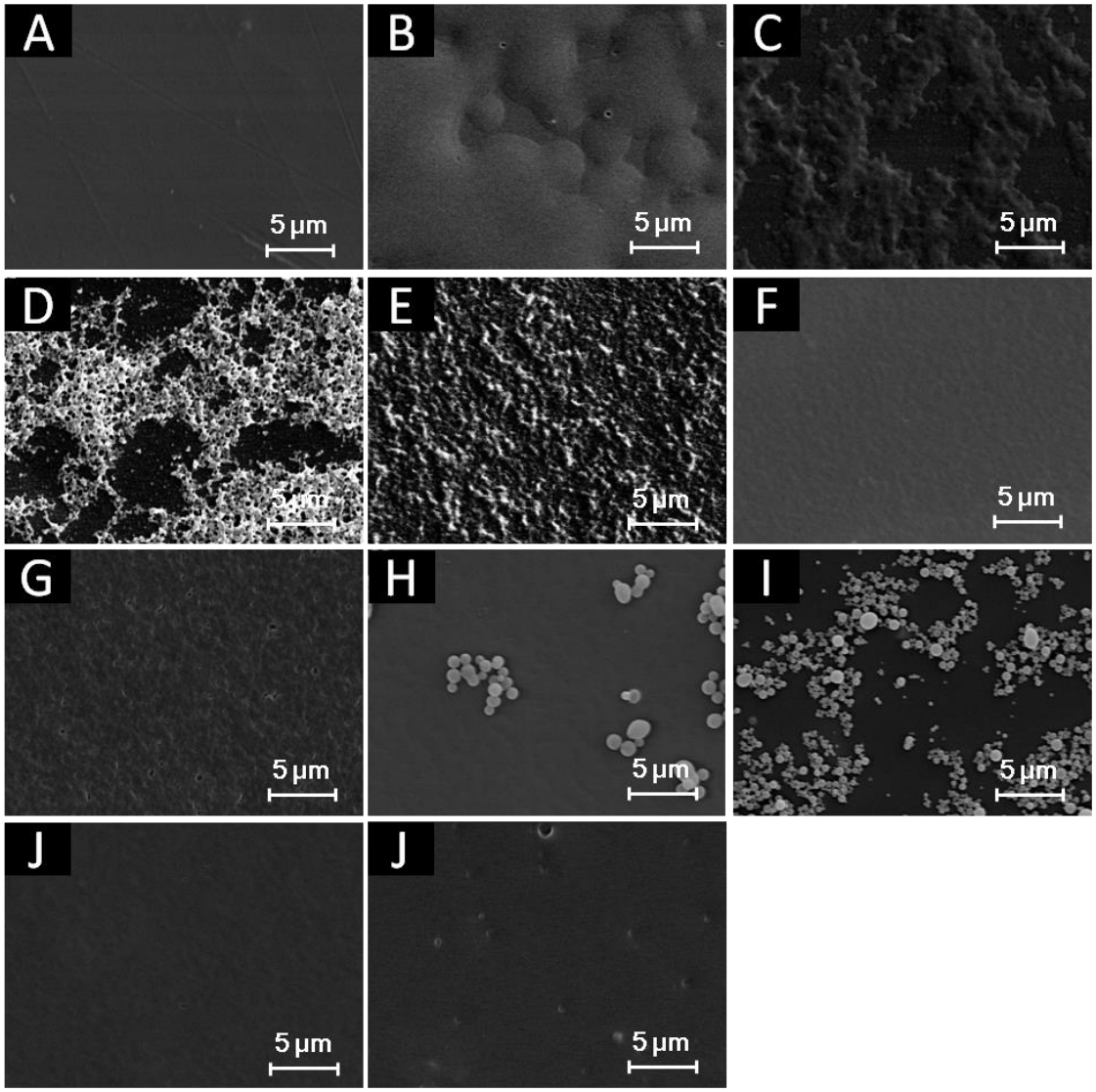

Figure 1-14. Representative SEM images of each polymer film prepared under dry conditions. Substrate = PET sheet. (A) PET surface, (B) lin-PHEMA 27k, (C) lin-PHEMA 290k, (D) star-PHEMA, (E) star-H71M29, (F) star-H47M53, (G) star-H22M78, (H) lin-PMMA 10k, (I) star-PMMA, (J) lin-Block, (K) lin-Random.

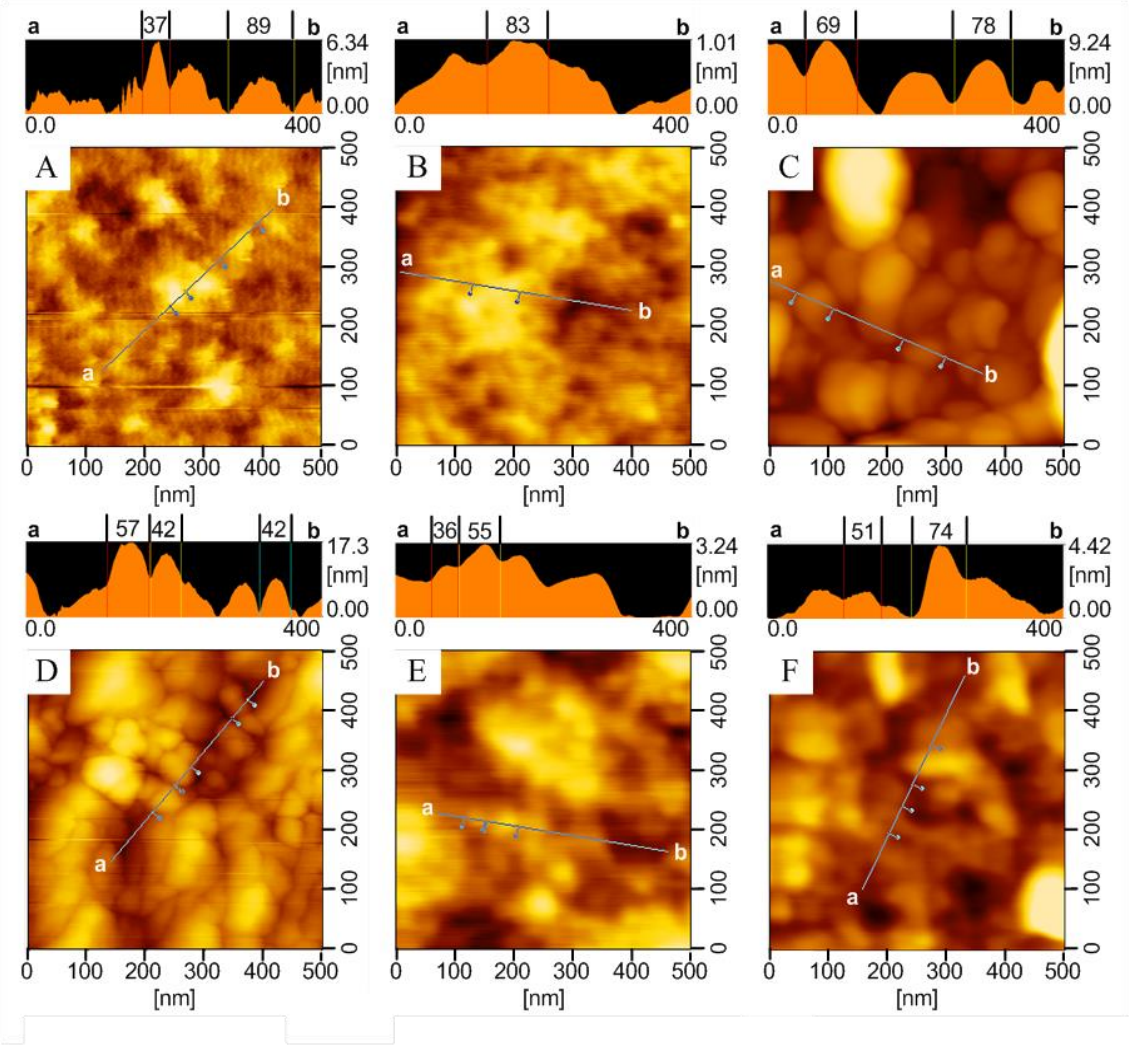

Figure 1-15. Representative AFM images of each polymer film prepared under dry conditions. Substrate = PET sheet. (A) PET surface, (B) lin-PHEMA 27k, (C) star-PHEMA, (D) star-H47M53, (E) star-PMMA, (F) lin-Block.

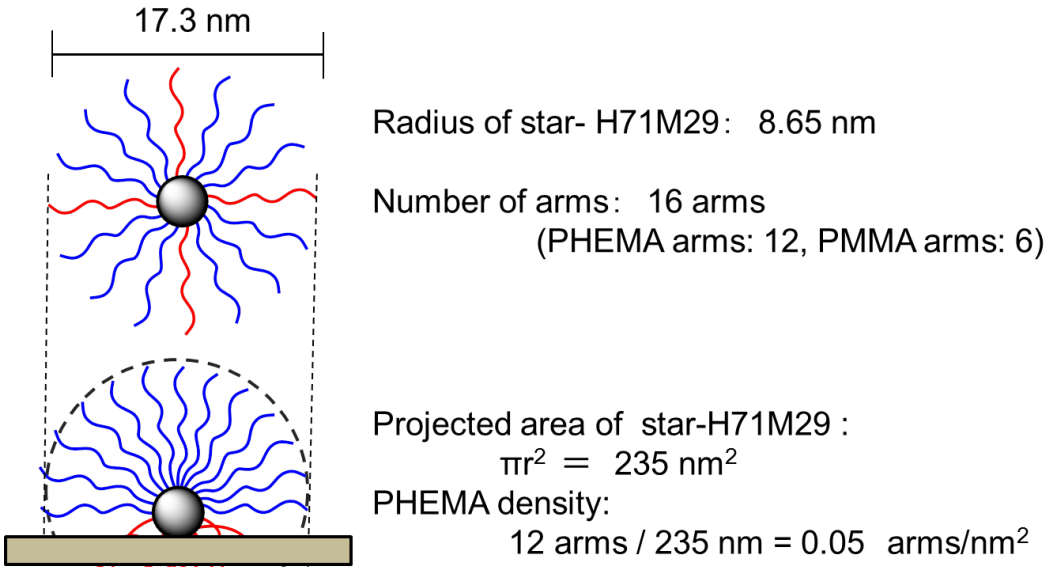

Figure 1-16. Comparison images of the hydrated lin-PHEMA-coated surface and star polymer-coated surface.

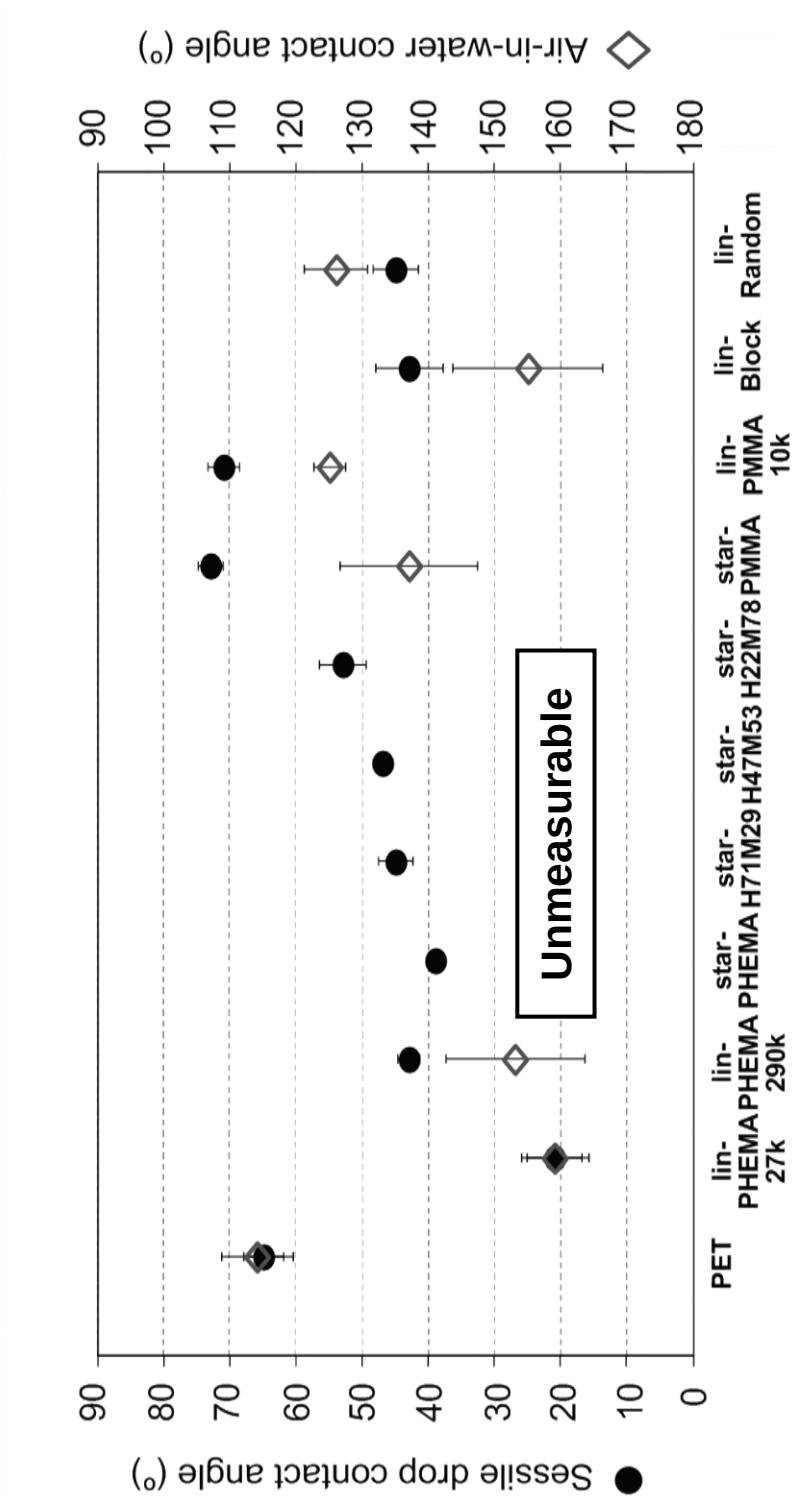

Figure 1-17. Contact angles of the water droplets (sessile drop) and air-in-water (captive bubble drop) on the polymer-coated surfaces.

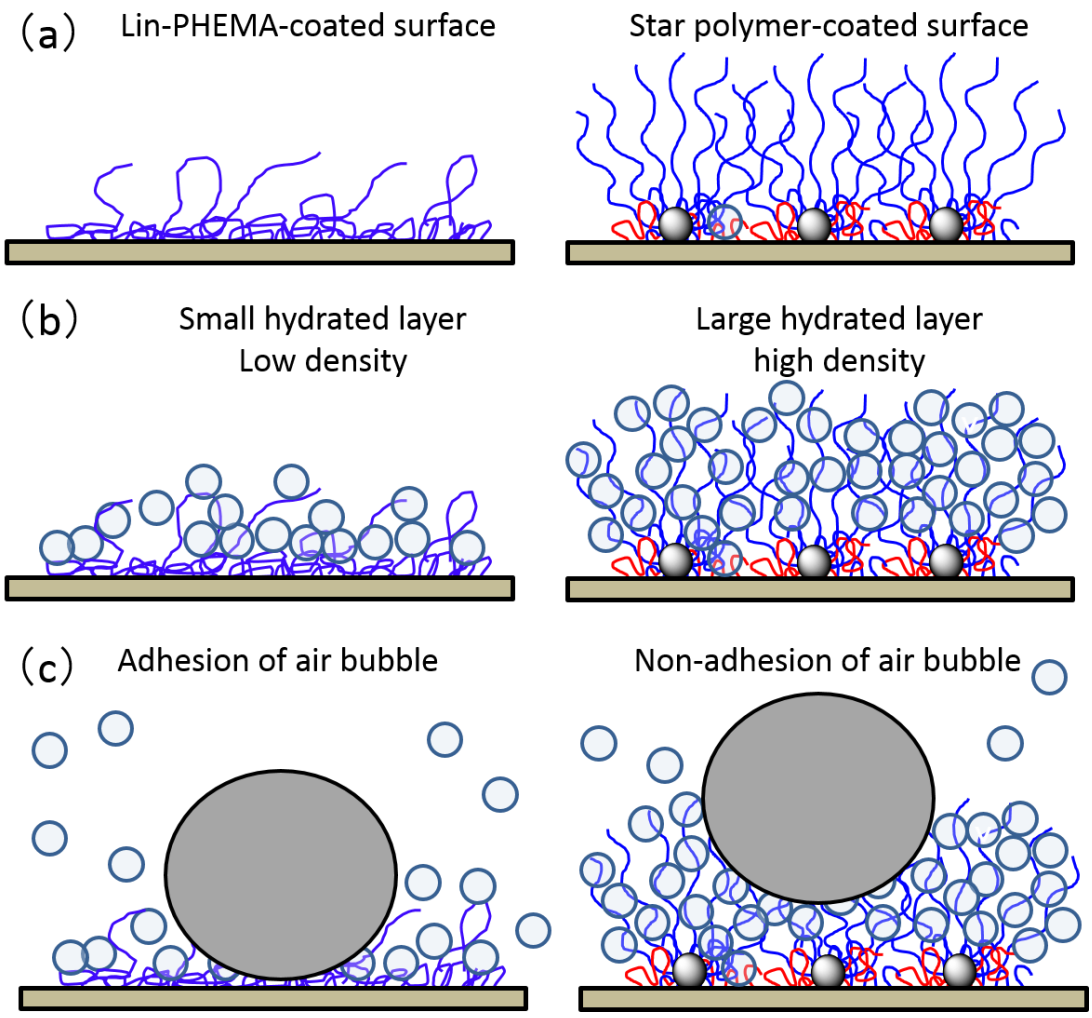

Figure 1-18. Comparison images of the hydrated lin-PHEMA-coated surface and star polymer-coated surface.

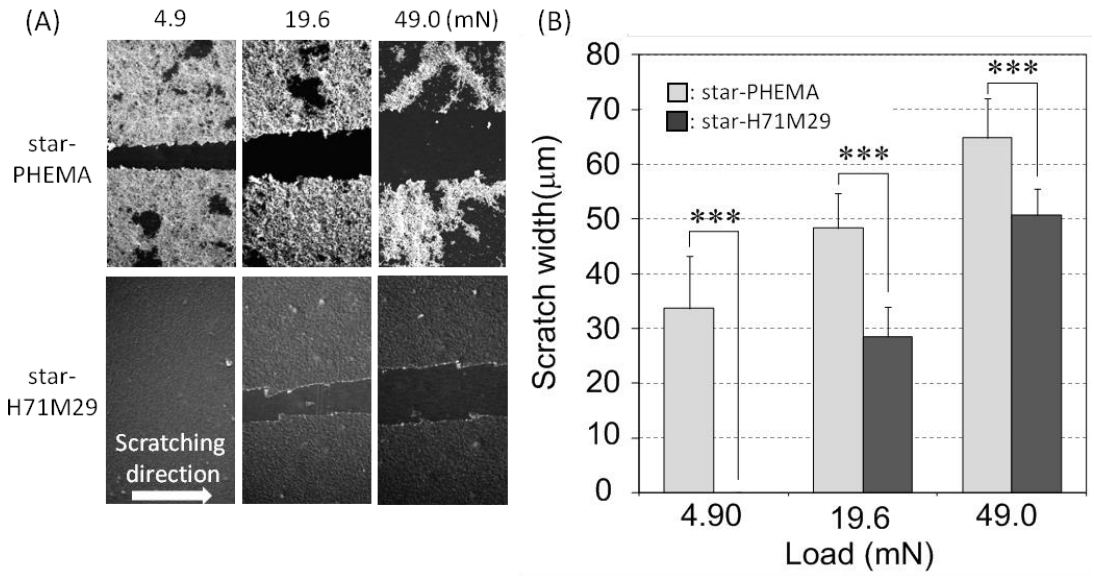

Figure 1-19. Scratch resistance test. (A) SEM of star-PHEMA and star-H71M29 coatings at the different scratch loads. (B) Scratch widths after loads on star-PHEMA and star-H71M29 coating surfaces (mean ± standard deviation, $n = 3$). ***$p < 0.001$.

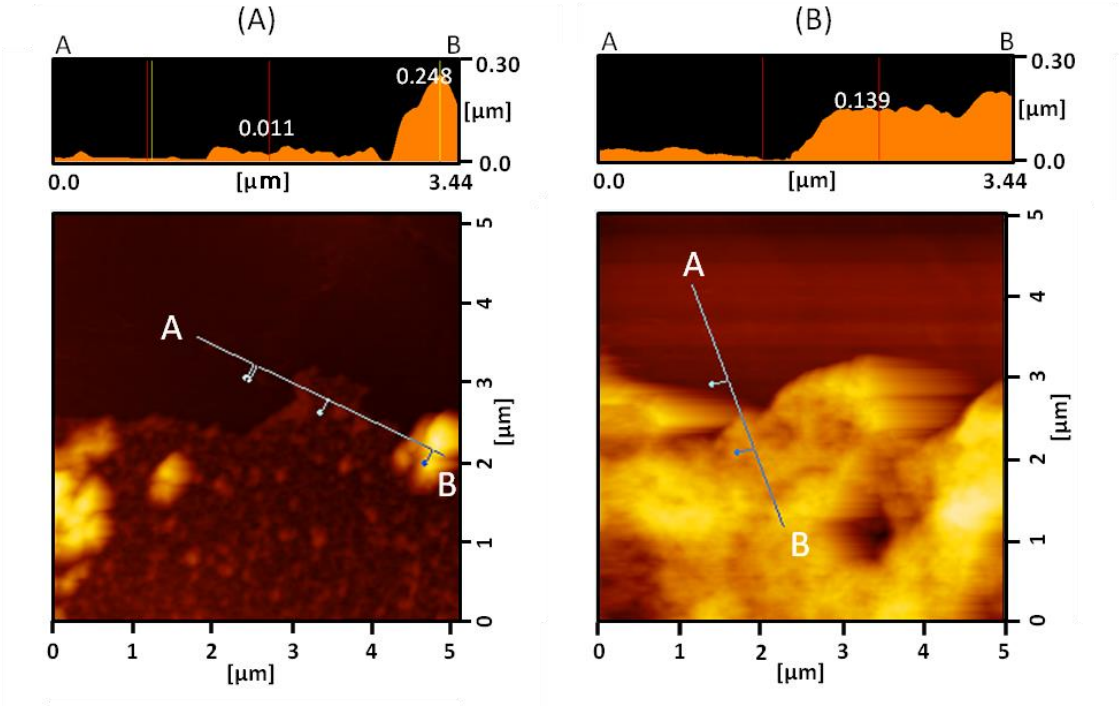

Figure 1-20. Surface characterization after scratch testing. AFM images of edge of scratch on (A) star-PHEMA and (B) star-H71M29 coated surfaces.

CHAPTER 2

Resistance to platelet adhesion

CHAPTER 2

Resistance to platelet adhesion

2-1. Introduction

Despite the wide use of biomaterials in medical application, the biocompatibility of artificial organs materials are still not enough from foreign body reactions, which are triggered when the medical devices contact directly with tissue and/or blood. In general, it was known that rapid adsorption of plasma proteins occurs on the foreign surfaces first, followed by platelet adhesion which triggers the coagulation of blood due to thrombus formation. Fibrinogen and von Willebrand factor (vWF) in blood plasma are particularly important for platelet adhesion, where adsorbed fibrinogen can readily facilitate platelet adhesion and activation. Integrin αIIbβ3 (GPIIb/IIIa) is most abundant glycoprotein on the platelet surface. The affinity of this integrin to its ligands, most notably fibrinogen and vWF is highly modulatable, and on activation it mediates platelet adhesion, aggregation, and spreading on foreign material surface (Figure 2-1, 2-2) [1]. So, antithrombogenic

material surface should suppress platelet adhesion.

As previously mentioned in general introduction, hydrophilic polymer brush structure reported the beneficial resisting protein adsorption. I demonstrated that the build highly dense graft-like surface using star polymer coatings.

In this chapter, I demonstrated anti-adhesion activity of star polymer coatings using platelets. Both star-PHEMA and star-H71M29 prevented platelet adhesion more effectively than the linear PHEMA. This result shows that denser hydrophilic polymer coated surfaces more suppress the platelet adhesion, suggesting that star polymer coated-surface has high density graft-like architecture which was resisting protein adsorption cause of platelet adhesion.

2-2. Materials and Methods

2-2-1. Materials

Water used in this work was pure water from a Milli-Q (18 MΩ-cm) system. Poly(ethylene terephthalate) (PET) film (FS2000, Futamura Kagaku K.K., Osaka, Japan) was cleaned by sonication in 0.45 μm-filtrated ethanol for 30 min, and then dried

under vacuum for overnight. All polymer solution samples were filtrated using a PTFE filter (pore size = 0.45 μm) before casting. The polymer solutions (25 μL, 0.1 mg/mL) were dropped on PET films (1.0 cm × 1.0 cm), evaporated at room temperature, and then dried under reduced pressure overnight. For the platelet adhesion assay, the coated films were cut into four pieces (0.5 cm × 0.5 cm). Whole blood was drawn from a healthy volunteer.

2-2-2. Platelet adhesion

The fresh blood containing 0.1% sodium citrate as a anticoagulant was centrifuged at 800 rpm for 5 min, and the obtained supernatant, platelet rich plasma (PRP), was diluted three times with Dulbecco's phosphate buffered saline (PBS). The polymer coated PET films were fixed in a weighing bottle (diameter 3.5 cm) using a small amount of adhesive compound (bath-bond Q, Konishi co., Ltd, Osaka, Japan). Methanol was added to the bottle for 10 min to swell the PHEMA arm, and then the polymer-coated surface was washed with Milli Q water three times, and finally placed in PBS. To the weighing bottle, 1.5 mL of the diluted PRP was added and then

incubated at 37 ºC for 30 min under a humid atmosphere. After washing with PBS three times, the adhered platelets were fixed in 2% glutaraldehyde PBS solution at 4 ºC for 2 h. The samples were washed with PBS three times, once with water and once with acetone, and then dried under vacuum overnight.

All samples were sputter-coated with gold using VPS-020 Quick Coater (ULVAC KIKO, Ltd., Miyazaki, Japan) prior to scanning electron microscope (SEM, S-4800, Hitachi, Tokyo, Japan) observation. The number of the adhered platelets on the polymer-coated surfaces was counted using SEM images at an accelerating voltage of 15 kV and at a magnification of 4×10^2. At least three readings on different parts of a sample were averaged. The presented data are the average values of three samples. Errors were determined through evaluation of the standard deviation of the measurements.

2-2-3. Stability test

Each polymer-coated PET substrate was fixed on the bottom of a 50 mL vial. PBS (20 mL) or 0.5 wt% Triton X-100 in PBS (20 mL) was added into the vials. The vials

were capped and incubated at 37 ºC with shaking at 180 rpm for 7 days. The substrates were washed with Milli-Q (20mL) five times. The sample's stability was evaluated by the platelet adhesion assay described above.

2-2-4. Statistical Analysis

Statistical analysis of the differences between groups was performed using the analysis of variance (ANOVA) followed by Dunnett's test. All values for platelet adhesion are expressed as mean ± standard deviation.

2-3. Results and Discussion

2-3-1. Platelet adhesion

To assess anti-adhesion activity of the star polymers, I examined *in vitro* platelet adhesion to the coated surfaces. The coated PET substrates were soaked in water for 12 hours prior to the platelet adhesion assay to hydrate the polymer coatings and increase the surface hydrophilicity as indicated by the air-bubble contact angle

measurement discussed in Chapter 1. The polymer-coated PET substrates were incubated with platelet rich plasma (PRP) at 37 °C for 30 min, based on the standard protocol in the literature [2]. The platelet adhesion on the coated surfaces was characterized by SEM. The numbers of platelets adhered to star-PHEMA and star-H71M29 coatings were significantly smaller than those of the non-coated PET and other star and linear polymers. The magnified SEM images indicated that the morphology of platelets adherent on the surfaces depended on the coated polymers. Some platelets formed lamellipodia on the non-coated PET surface, which resulted in aggregation of platelets to adhere firmly onto the surface. On the other hand, each platelet seems isolated rather than aggregated for most of the polymer coatings.

To quantify the platelet adhesion, the numbers of adherent platelets on the coatings were determined from the SEM images (Figure 2-3, 2-4). It is evident that the numbers of platelets (Figure 2-5) on the coating of star-polymers, except the star-PMMA, were significantly smaller than non-coated PET. The percentages of inhibition were 78% for the star-PHEMA, 23% for lin-PHEMA 27k and 43% for lin-PHEMA 290k (Table 2-1). These results indicate that star-PHEMA prevented platelet adhesion more effectively than linear PHEMA. This seems to reflect higher hydrophilicity of star-PHEMA than lin-PHEMA, which was determined by the

air-bubble contact angle in water. These results also suggest that the star-shaped polymer architecture plays an important role in resistance to platelet adhesion. The polymer brush-like structures by star polymer architecture are likely to be expanded in water, which increases the hydrophilicity of coatings as well as the exclusion volume of polymer brushes, expelling platelets more effectively than linear polymers. However, rough surfaces generally favor platelet adhesion because of increased areas available for adhesion as well as geometrical niches for adhesion mechanisms [3,4]. Therefore, the fibrous network structure of star-PHEMA coating could rather favor the platelet adhesion. I speculate that the fibrous network is hydrated and swollen with water, which increases the coverage of coatings and reduces the surface roughness, contributing to high hydrophilicity and thus high anti-adhesion activity.

The coatings of heteroarm star polymers also showed an inhibitory effect against platelet adhesion. The star-H71M29 showed a similar anti-adhesion activity to star-PHEMA. However, some platelets on the star-H71M29 coated surface were in non-activated form. The difference may be arisen from the amount and activation degree of proteins adsorbed on the star-H71M29-coated surface (Figure 2-6). In the future, these mechanisms should be cleared. The number of adhered platelets increased as the percentage of PMMA arms in the star polymers increased. This

indicates the polymers containing more hydrophobic PMMA are less resistant to platelet adhesion. The block copolymer lin-Block showed a similar level of anti-adhesion activity as compared to the star polymer coatings, whereas the random copolymer lin-Random showed no significant anti-adhesion activity. The PMMA segment of the block copolymer is likely to increase the adhesion of polymer chains to the PET surface, anchoring the hydrophilic PHEMA segment, which provide polymer brush-like structure, and prevent platelet adhesion. It has also been reported that polymer coating on a glass surface by amphiphilic copolymers such as triblock copolymer consisting of PHEMA and hydrophobic polystyrene (PSt) (PHEMA-*b*-PSt-*b*-PHEMA) effectively prevented adhesion of platelets and filopodium [5]. Block copolymers with fluoroalkyl components also showed anti-fouling and fouling-release activities against proteins. These studies suggest that formation of phases-separated domains by the hydrophilic and hydrophobic (fluorinated) polymers are responsible for the anti-adhesion activity because these domains may disrupt settlement of protein and microbial adhesion [6].

2-3-2. Stability of coatings in aqueous environment

Since the polymers used in this study are not covalently bound onto PET surface, the polymers might be released into water or the coatings delaminated, exposing the bare PET surface after a prolonged time period. This would compromise the anti-adhesion activity of coatings against platelets. To that end, the coating stability was assessed by incubating the coatings in PBS or surfactant (Triton X-100) solution for 7 days at 37°C with gentle shaking at 180 rpm prior to the platelet adhesion test. Star-PHEMA and star-H71M29 coatings retained good anti-adhesion effect against platelets even after the surfactant challenge (Figure 2-7). The lin-PHEMA 290k and 27k and lin-Block showed the same level of percentages of inhibition as compared to the same samples tested previously, shown in Figure 2-6. The percentage of inhibition by the star polymer coatings (96-97%) slightly increased from those of the same samples without incubation (78-88%) (Table 2-1). The slight enhancement of the anti-adhesion activity may be related to the hydration of coated polymer chains in water during the incubation for 7 days, increasing the hydrophilicity of coatings.

2-4. Conclusion

Among the star polymers, star-PHEMA and star-H71M29 inhibited adhesion of platelets by 78-88% relative to non-coated PET surface. These coatings retained the anti-adhesion properties after incubation in PBS or surfactant solution for 7 days, suggesting that the star polymer architecture provided high polymer chain density on the surfaces to prevent adhesion of platelets as well as coating stability to prevent exposure of bare PET surfaces. The results indicate that star polymers can provide an effective approach to the preparation of high density polymer brushes on PET surfaces for anti-adhesion coatings against platelets.

The polymer preparation and coating method are simple and cost-effective. PET was used as a model substrate in this work but this star polymer coating can be used with a wide range of biomedical synthetic materials. It has been reported that dopamine derivatives were used to modify inert plastic and metal surfaces with chemically labile groups for polymer modifications, providing versatile methods for surface modification and antithrombogenic coatings. Similarly, I envision that the star polymer coatings may provide a new strategy for polymer brush coatings for many different types of surface.

2-5. References

[1] Varga-Szabo D, Pleines I, Nieswandt B. Cell adhesion mechanisms in platelets. Arterioscler Thromb Vasc Biol 2008;28:403-412.

[2] Xu GC, Hibino Y, Suzuki Y, Tanihara M, Imanishi Y, Awazu K. Free electoron laser induces specific immobilization of heparin on polysulfone films. J Biomater Sci Polym Edn 2001;12:503-14.

[3] Koh LB, Rodriguez I, Venkatraman SS. The effect of topography of polymer surfaces on platelet adhesion. Biomaterials 2010;31:1533-45.

[4] Hulander M, Lundgren, Faxalv L, Lindahl TL, Palmquist A, Berglin M, Elwing H. Gradients in surface nanotopography used to study platelet adhesion. Colloids Surf B: Biointerfaces 2013;110:261-9.

[5] Nagaoka S, Nakao A. Clinical application of antithrombogenic hydrogel with long poly(ethylene oxide)chains. Biomaterials 1990;11:119-21.

[6] Banerjee I, Pangule RC, Kane RS. Antifourling coatings: Recent developments in the design of surfaces that prevent fouling by protein, bacteria, and marine organisms. Adv Mater 2011;23:690-718.

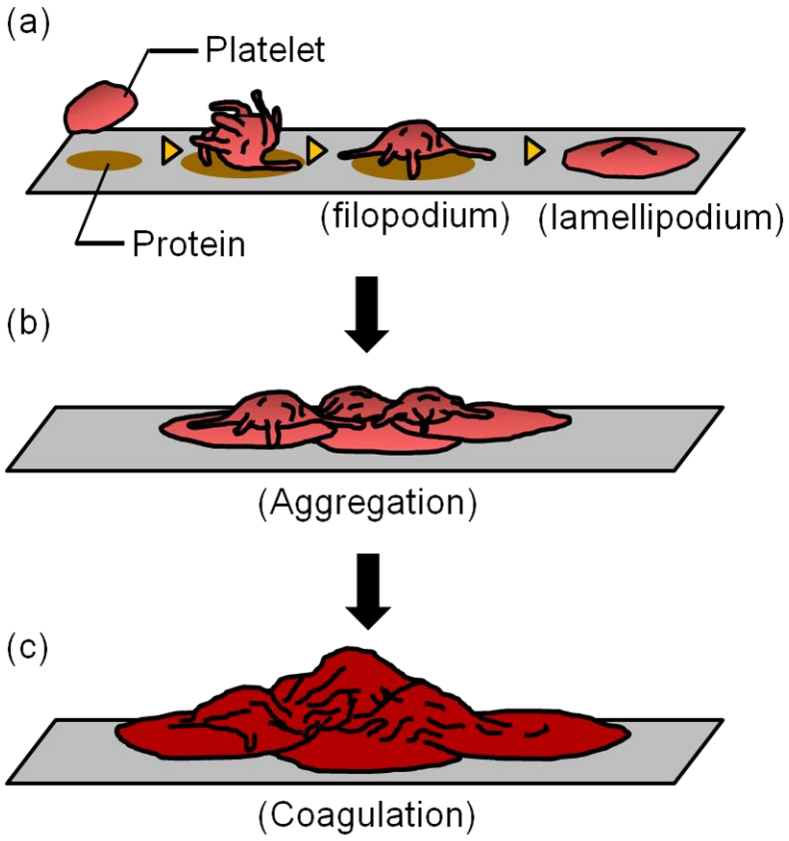

Figure 2-1. Platelets adhesion and formation of coagulation on the foreign material surface (Figure 5, vascular illness, web site of circulatory organs disease information service.)

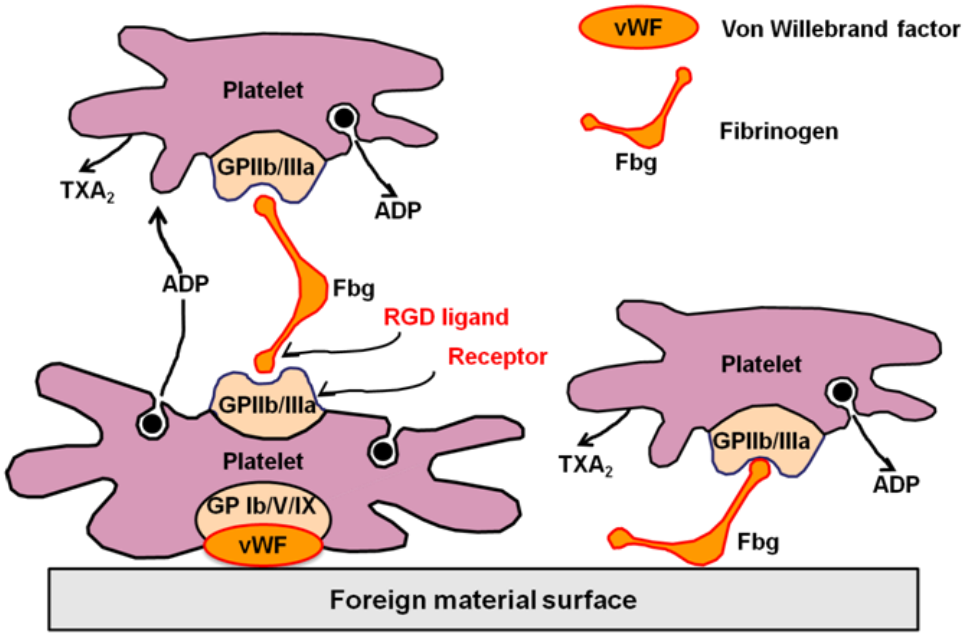

Figure 2-2. Platelet adhesion and formation of coagulation.

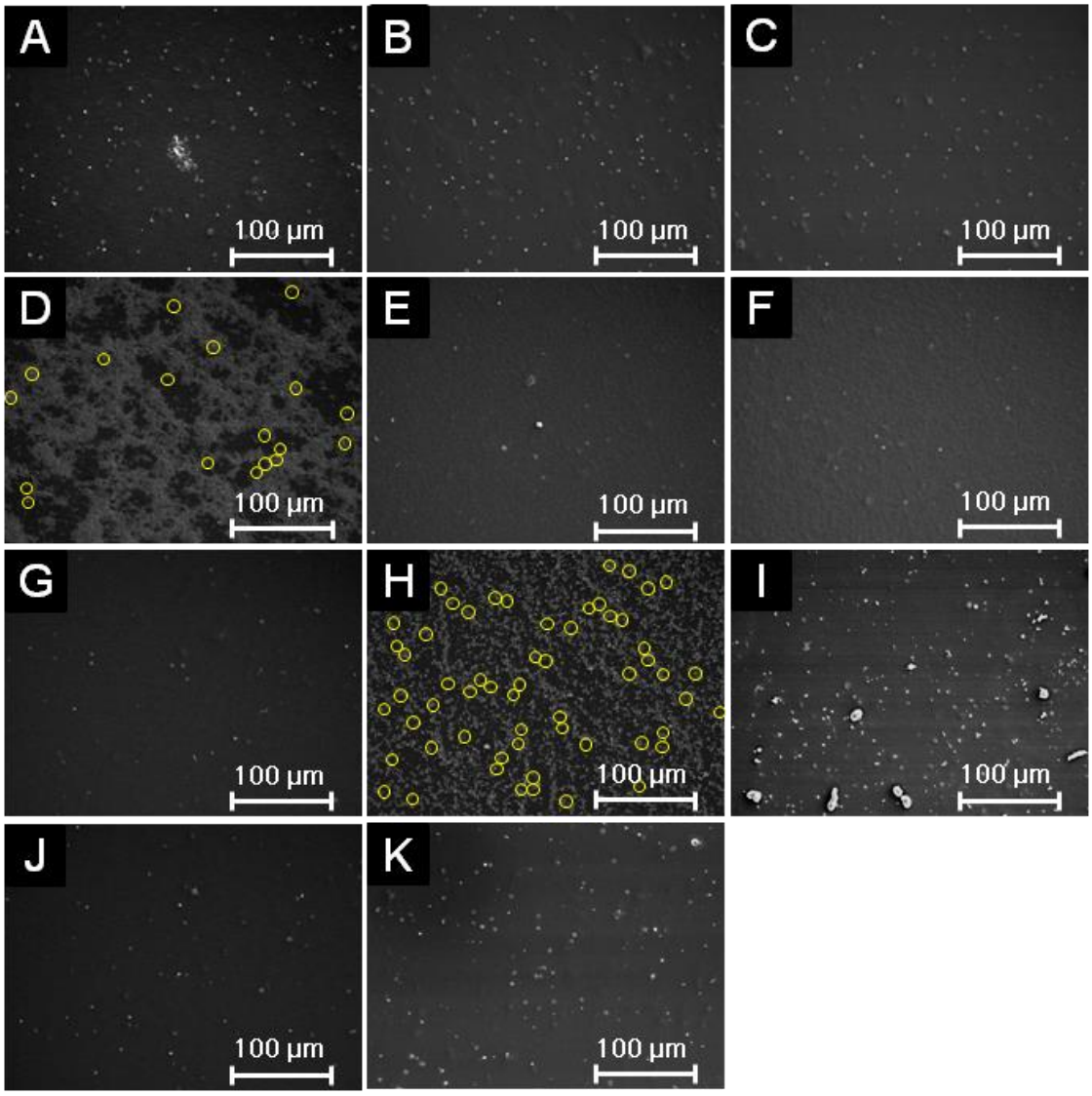

Figure 2-3. Adherent platelet images on each polymer surface. Substrate = PET sheet. Incubation = PRP, 37 ºC, 30 min. Image magnification = × 400; (A) PET surface, (B) lin-PHEMA 290k, (C) lin-PHEMA 27k, (D) star-PHEMA, (E) star-H71M29, (F) star-H47M53, (G) star-H22M48, (H) star-PMMA, (I) lin-PMMA 10k, (J) lin-Block, (K) lin-Random.

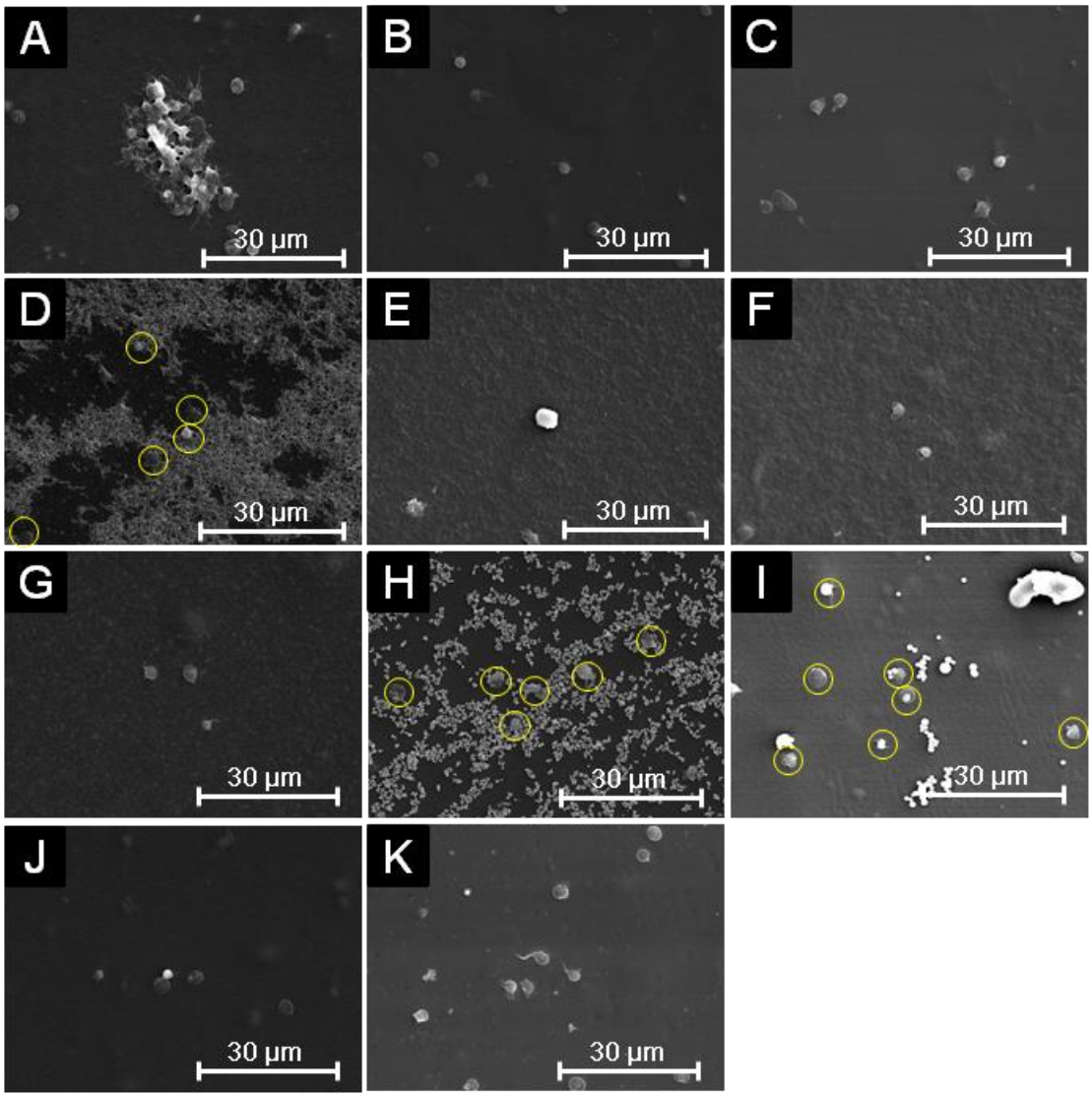

Figure 2-4. Adherent platelet images on each polymer surface. Substrate = PET sheet. Incubation = PRP, 37 ºC, 30 min. Image magnification = × 1500; (A) PET surface, (B) lin-PHEMA 290k, (C) lin-PHEMA 27k, (D) star-PHEMA, (E) star-H71M29, (F) star-H47M53, (G) star-H22M48, (H) star-PMMA, (I) lin-PMMA 10k, (J) lin-Block, (K) lin-Random.

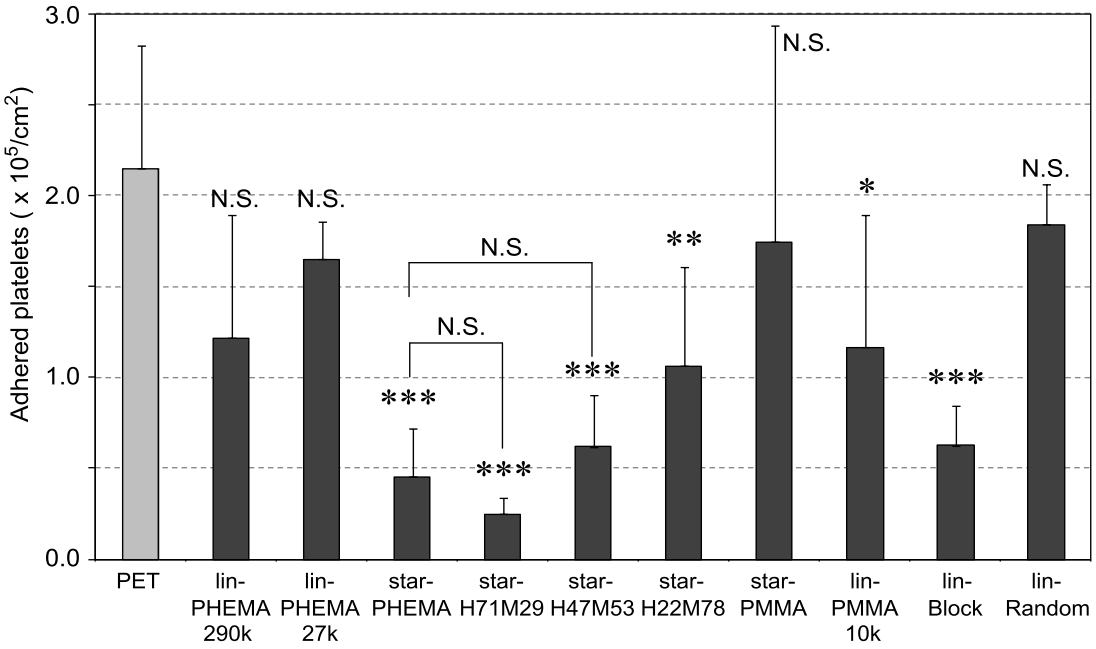

Figure 2-5. Numbers of adhered platelet on the material surfaces. ***$p < 0.001$, **$p < 0.01$, *$p < 0.05$ vs. PET, mean ± standard deviation, $n = 3$.

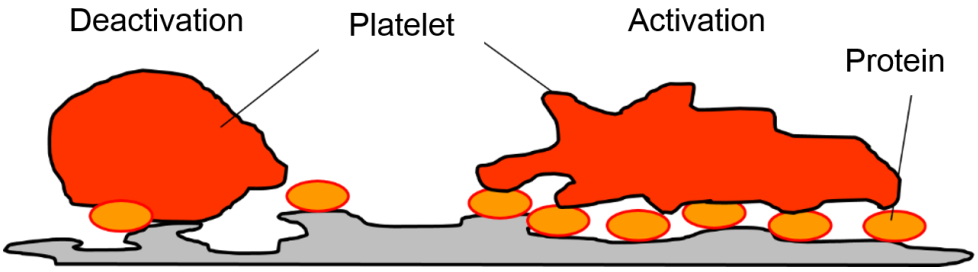

Figure 2-6. Comparison of deactivation and activation form of adherent platelets.

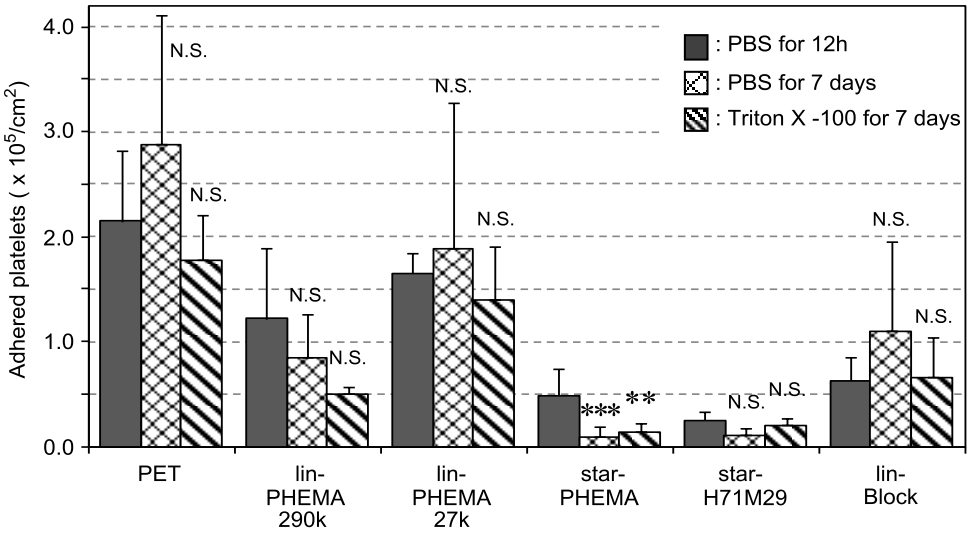

Figure 2-7. Stability test of polymer-coated surface by platelets adhesion to the coatings after incubation in PBS for 12 h, and subsequently in PBS or 0.5 wt% Triton X-100 solution with gentle shaking for 7 days. ***p ＜0.0001, **p ＜0.001, *p ＜ 0.005 vs. PET.

Table 2-1. Summary of inhibition activity of polymers against adhesion of platelets.

Polymers	Inhibition percentage (%)		
	Standard test	Stability in PBS (7 days)	Stability in Triton X-100 (7 days)
lin-PHEMA 290k	43±27	71±16	71±3
lin-PHEMA 27k	23±8	35±48	26±23
star-PHEMA	78±11	97±3	92±5
star-H71M29	88±1	96±1	88±3
lin-Block	71±7	56±27	63±21

a) The percentage of inhibition was calculated by the following equation: % of inhibition = (Adherent Platelet on PET – Adherent Platelet on polymer coatings)*100/ Adherent Platelet on PET. b) Coatings incubated in PBS for 12 hours prior to the test, calculated based on the date from Figure 2. c) Coatings incubated in PBS for 7 days prior to the test. d) Coatings incubated in 0.5wt% Triton X for 7 days prior to the test.

CHAPTER 3

Inhibition of bacterial adhesion

CHAPTER 3

Inhibition of bacterial adhesion

3-1. Introduction

Bacterial infections related to biomedical polymer surfaces of artificial organs, such as artificial blood vessels, artificial valves, catheters and ventricular assist device, are a significant problem which cause serious complications after surgery and lead to failure of implants [1]. The three major types of prosthetic vascular grafts (arteriovenous, femoropopliteal, and aortic) differ with regard to the associated rates of infection and the most pertinent complications. More than 5 percent of arteriovenous grafts become infected [2]. These infections are associated with adhesion of bacteria to and colonization on implant surfaces, subsequently resulting in biofilm formations. Bacterial biofilms form robust biopolymer matrices, protecting bacteria from antibiotic challenges and contributing to resistance development. There is a need for surface coatings to prevent biofilm formation.

Anderson and associates reported that adhesion of *Staphylococcus epidermidis* (*S. epidermidis*) to a hydrophobic polymer, polyethylene, examined under well defined

shear conditions approximating those in the human blood circulation, is mediated by contact activated platelets, and not by adsorbed proteins. In their study, more than 50 % of adherent bacteria were bound to platelets [3].

Furthermore, *S. epidermidis* produces several proteins which specifically bind to proteins of the extracellular matrix including fibronectin, fibrinogen, vitronectin and collagen [4].

To that end, it is interested to develop hydrophilic surfaces using polymer coatings for artificial organ surfaces in order to reduce bacteria adhesion. Hydrophilic surfaces are known to reduce protein and bacterial adhesion [5-8]. Surfaces with high density hydrophilic polymers were previously prepared by polymerization from initiators on the surface (graft polymerization). Such surfaces displayed resistance to protein adsorption likely due to their high mobility and the excluded volume effect of polymer chains such as poly(ethylene oxide) (PEO) and poly(2-hydroxyethyl methacrylate) (PHEMA) [9-11]. Although this approach of dense polymer chains would be promising for new anti-fouling surfaces, it is difficult to realize graft polymerization on conventional implant materials such as PET and PU.

In this study, I already studied resisting platelet adhesion on the star polymer coated surfaces in Chapter 2. The star-PHEMA and star-H71M29 (PHEMA /

poly(methyl methacrylate) (PMMA) = 71/29 mol%). I prepared polymer coatings and evaluated their anti-biofim activity against *Escherichia coli* (*E. coli*) for 20 h. The inhibition of bacterial adhesion was evaluated using luminescent assay and scanning electron microscope (SEM) images.

3-2. Materials and Methods

3-2-1. Materials

Materials basically used in this chapter are the same as described in Chapter 2. *E. coli* (ATCC® 25922™), Muller-Hinton II (MH) broth (Becton, dickinson and company), Bac Titer-Glo™ microbial cell viability assay (Bac Titer-Glo™) (Promega).

3-2-2. Bacterial adhesion

A polymer-coated film was fixed to the bottom of wells in a 24-well culture plate using a small amount of silicon adhesive compound, and dried under reduced pressure overnight. The polymer-coated surfaces were washed with Milli-Q water three times, and finally immersed in PBS at 37 ºC for 12 h for hydration. *E. coli* (ATCC® 25922™) was grown in MH broth (5 mL, pH = 7.4) at 37 ºC overnight. The

cells diluted with MH broth to give OD_{600} = 0.1 was incubated at 37 ºC and 180 rpm for 90 min. The bacterial culture in the midlogarithmic phase (OD_{600} = 0.5-0.6) was washed three times with MH broth by centrifuging 5 mL of the culture at 3,700 rpm for 5 min, and re-suspended in 10% MH broth in distilled water adjusted to OD_{600} = 0.003. Bacterial suspension (2.0 mL) was added to each well and incubated at 37 ºC for 20 h. After the incubation, the OD_{590} of supernatants were measured by a microplate reader as a measure of bacterial growth. The supernatant was removed from the well, and the polymer-coated substrates were rinsed with PBS three times to remove non-adherent planktonic bacteria. The substrates with adhered bacteria were transferred to a new 24-well plate to quantify only the bacteria adherent to the substrate, because bacteria might non-specifically adhere to a well wall of the assay plate incubated with bacteria. After removing PBS, 10% Bac Titer-Glo™ in PBS (500 μL) was added to the bacteria adhered to the coatings and incubated for 5 min at room temperature. The incubated Bac Titer-Glo™ solution was transferred to a 96-well white microplate, and the luminescence from the solutions were measured to determine the viability of the adherent bacteria.

3-2-3. SEM images of adherent bacteria

Adherent bacteria on the polymer-coated surfaces were prepared by the same method as the bacterial adhesion assay described above. The polymer coatings were incubated with bacteria at 37 ºC for 20 h, and the adhered bacteria were fixed by 2% glutaraldehyde in PBS solution at 4 ºC for 2 h. The samples were washed with PBS and water three times, and dried under vacuum overnight. All samples were observed in the same procedure as the platelet adhesion described in Chapter 2.

3-2-4. Statistical Analysis

Statistical analysis of the differences between groups was performed using the analysis of variance (ANOVA) followed by Dunnett's test. All values for platelet adhesion are expressed as mean ± standard deviation.

3-3. Results and Discussion

3-3-1. Bacterial adhesion

Biomedical synthetic materials suffer from bacterial adhesion and subsequent biofilm formation, causing adverse infections and complications (Figure 3-1). To evaluate the resistance of polymer coatings to bacterial adhesion, we used *E. col*i as an initial model bacterium. *E. coli* is one of the pathogens causing adverse device- and implant-associated infections. In general, the results are similar to those of platelet adhesion. *E. coli* formed dense bacterial clusters on the unmodified PET surface (Figure 3-2, 3-3). These bacterial clusters are considered to be adhered strongly on the surfaces because the non-adherent and lightly adherent bacteria on the surface were washed away with PBS 3 times after the incubation, and only strongly adhered bacteria can remain on the surface. The star-PHEMA and star-H71M29 coatings showed few bacteria. The E. coli appears to adhere on the top of the network structure of the star-PHEMA coating rather than being trapped or in varied positions in the network. This may support the notion that the polymer network is swollen with water and covers

the coating surface, preventing bacterial adhesion to the empty spaces in the network. The adherent bacteria were quantified by the luminescence assay (Figure 3-4). It should be noted that there is no significant difference in the OD of the bacterial assay solutions incubated with the coatings, indicating that these polymer coatings did not inhibit bacterial growth in the solution. This suggests that inhibiting bacterial growth or killing bacteria is not the primary mechanism of these coatings' resistance to bacterial adhesion. Star-PHEMA and star- H71M29, and lin-PHEMA 27k and lin-Block showed a similar level of bacterial adhesion inhibition, although the lin-PHEMA 290k polymer did not prevent platelet adhesion (Table 3-1). These results indicate that the high-density polymer brushes on the coating surface effectively prevent E. coli adhesion. Similar to the platelet adhesion, the bacterial adhesion increased as the percentage of PMMA in the star polymers was increased, indicating that more bacteria adhere to the coating with higher hydrophobicity. The electronically neutral and hydrophilic polymer blush exhibits the effective inhibition of the bacterial adhesion [12]. PHEMA chains of the star polymer coated on the surface are also electronically neutral and hydrophilic, and they thus showed the effective resistance to *E. coli* adhesion. In addition, the PHEMA chain does not have a D-mannose-like structure, which is the ligand of the adhesion in the fimbriae, and it prevents the adhesion mediated by the fimbriae.

3-4. Conclusion

The polymer coated surfaces of star-PHEMA and star-H71M29 were resistant to bacterial adhesion by 94-97% relative to non-coated PET as well as resisting platelet adhesion. The results indicate that star polymers can provide an effective approach to the preparation of high-density polymer brushes on PET surfaces for anti-adhesion coatings against platelets and bacteria. The polymer synthesis and coating preparation are facile compared to other methods for achieving hydrophilic surfaces. This method of surface coating is applicable for conventional artificial organs materials such as PET, as hydrophobic polymer chains mechanically attach to artificial organs materials and anchor the star polymers onto the surface.

3-5. References

[1] Didisheim P. Current concepts of thrombosis and infection in artificial organs. ASAIO Journal 1994;40:230-37.

[2] Darouiche RO. Treatment of infection associated with surgical implants. N Engl J Med 2004;350:1422-9.

[3] Weng IW, Anderson JM, Marchant RE. Staphylococcus epidermidis adhesion to hydrophobic biomedical polymer is mediated by platelets. J Infect Dis 1993;167:329-36.

[4] Mack D, Davies AP, Harris LG, Rohde H, Horstkotte MA, Knobloch JKM. Microbial interaction in *Staphylococcus epidermidis* biofilms. Anal Bioanal Chem 2007, 387, 399-408.

[5] Krishnan S, Weinman CJ, Ober CK. Advances in polymers for anti-biofouling surfaces. J Mater Chem 2008;18:3405-13.

[6] Martins MCL, Wang D, Ji J, Feng L, Barbosa MA. Alubmin and fibrinogen adsorption on PU-PHEMA surfaces. Biomaterials 2003;24:2067-76.

[7] Kiremitci-Gumusderelioglu M, Pesmen A. Microbial adhesion to ionogenic PHEMA, PU and PP implants. Biomaterials 1996, 17, 443-9.

[8] Mackintosh EE, Patel JD, Marchant RE, Anderson JM. Effects of biomaterial surface chemistry on the adhesion and biofilm formation of Staphyloccus epidermidis *in vitro*. J Biomed Mater Res A 2006;78A:836-42.

[9] Nejadnik MR, van der Mei HC, Norde W, Busscher HJ. Bacterial adhesion and growth on a polymer brush-coating. Biomaterials 2008;29:4117-21.

[10] Ayres N. Polymer brushes: Applications in biomaterials and nanotechnology.

Polym Chem 2010;1:769-77.

[11] Mrabet B, Nguyen MN, Majbri AM, Mahouche S, Turmine M, Bakhrouf A, Chehimi MM. Anti-fouling poly(2-hydroxyethyl methacrylate) surface coatings with specific bacteria recognition capabilities. Surf Sci 2009;603:2422-29.

[12] MacKintosh EE. Patel JD. Marchant RE. Anderson JM. Effects of biomaterial surface chemistry on the adhesion and biofilm formation of *Staphylococcus epidermidis in vitro*. J. Biomed. Mater. Res., Part A 2006;78: 836–42.

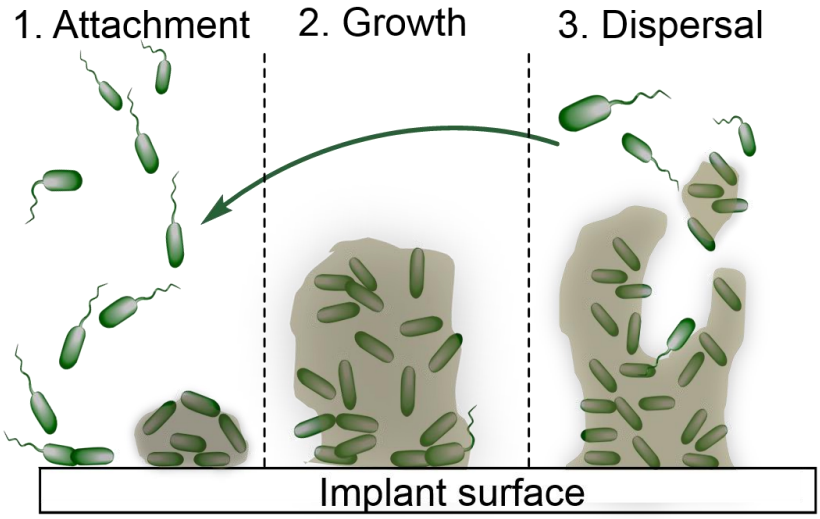

Figure 3-1. Bacterial adhesion and biofilm formation.

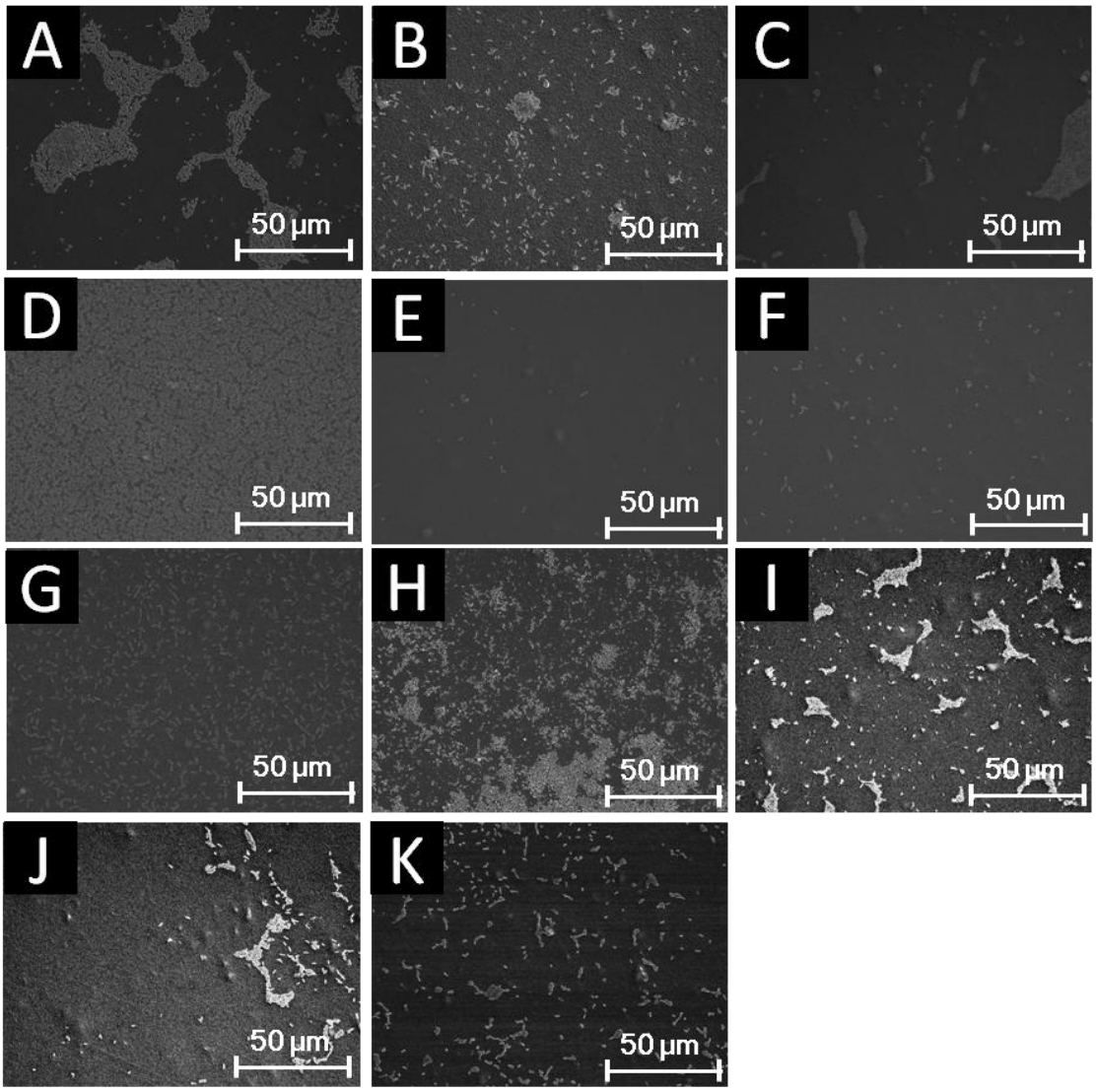

Figure 3-2. Adherent bacterial images on each polymer surface. Substrate = PET sheet; Incubation = *E. coli* in MH broth at 37 ºC for 20 h. Image magnification: × 400**;** (A) PET surface, (B) lin-PHEMA 290k, (C) lin-PHEMA 14k,(D) star-PHEMA, (E) star-H71M29, (F) star-H47M53, (G) star-H22M78, (H) star-PMMA, (I) lin-PMMA 10k, (J) lin-Block, (K) lin-Random.

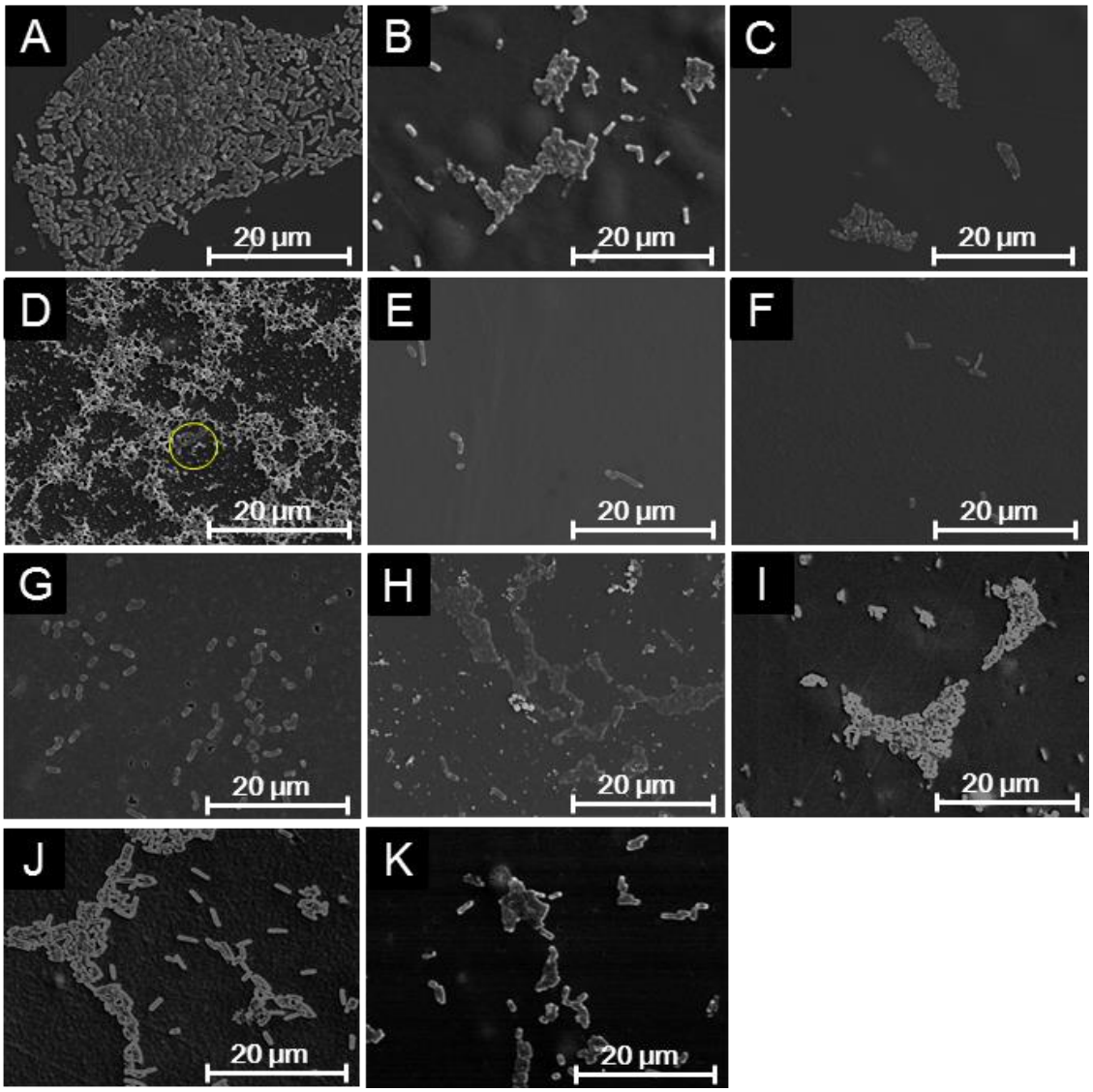

Figure 3-3. Adherent bacterial images on each polymer surface. Substrate = PET sheet; Incubation = *E. coli* in MH broth at 37 ºC for 20 h**.** Image magnification: × 1500; (A) PET surface, (B) lin-PHEMA 290k, (C) lin-PHEMA 14k,(D) star-PHEMA, (E) star-H71M29, (F) star-H47M53, (G) star-H22M78, (H) star-PMMA, (I) lin-PMMA 10k, (J) lin-Block, (K) lin-Random.

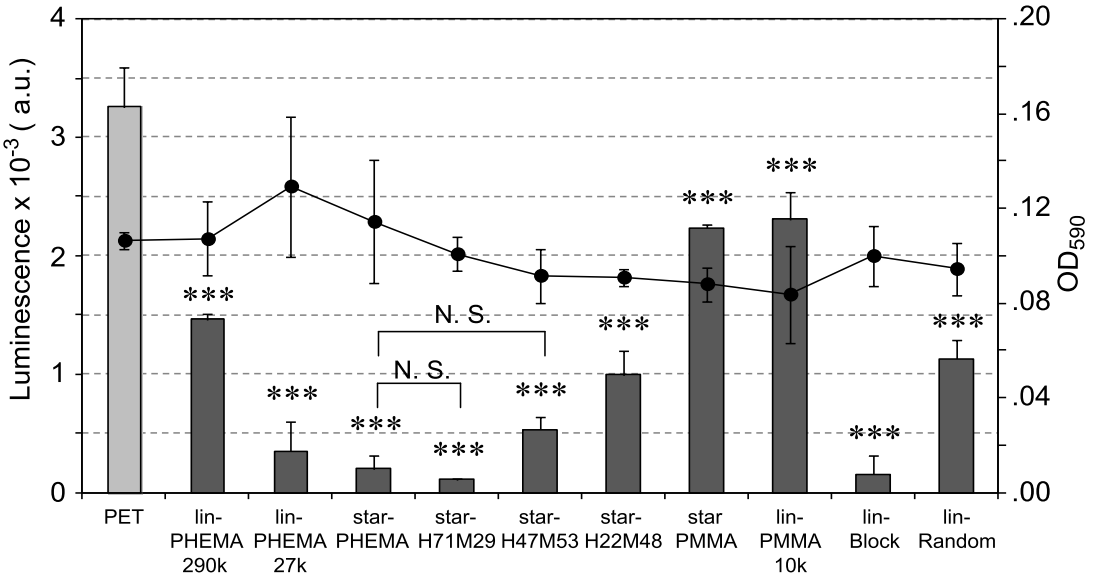

Figure 3-4. Bacterial adhesion, and growth in solution (mean ± standard deviation, n = 3). Adhesion of *E. coli* on to polymer-coated surface was quantified by a luminescence assay. The growth of E. *coli* was determined by OD_{590} (●) after 20 h at 37 ºC incubation. ***p ＜0.0001 vs. PET.

Table 3-1. Summary of inhibition activity of polymers against adhesion of bacteria.

Polymers	Inhibition percentage (%)
	E. coli
lin-PHEMA 290k	53±2
lin-PHEMA 27k	87±8
star-PHEMA	92±3
star-H71M29	94±1
lin-Block	93±5

a) The percentage of inhibition was calculated by the following equation: % of inhibition = (Bacterial luminescence on PET – Bacterial luminescence on polymer coatings)*100/ Bacterial luminescence on PET from Figure 3-4.

GENERAL CONCLUSION

Chapter 1 showed synthesis of heteroarm star polymers having both poly(2-hydroxyethyl methacrylate) (PHEMA) and poly(methyl methacrylate) (PMMA). It is known that both polymers were already used conventional medical devices such as contact lens. However, these polymers of linear or cross-linked gel were not enough antithrombogenic and antimicrobial activity. I focused on the hydrophilic polymer brush surfaces that were reported the antibiofouling activity such as resistance to protein adsorption in late years. However, it is difficult to graft polymers of high density on artificial organ surfaces which have low chemical reactivity. Additionally, a normal liner polymer coating method does not allow us to make highly dense brush surfaces. To achieve my goal, I devised the utilization of star polymers. The obtained heteroarm star polymers indicated that the arm compositions in different PHEMA/PMMA heteroarm star polymers were in agreement with the molar ratio of PTMSOEMA/PMMA in initial mixture. By systematically changing the molar ratios of PHEMA and PMMA heteroarm star polymers with different arm compositions were obtained. These star-PHEMA and heteroarm star polymers showed the most hydrophilicity assessed compared with lin-PHEMA by contact angles of captive bubble. This result may be stem largely from star polymer architecture.

Chapter 2 showed resisting platelet adhesion as an antithrombogenic activity on the star-PHEMA and star-H71M29 (PHEMA/PMMA = 71/29 mol%) coated surfaces. Among the star polymers, star-PHEMA and star-H71M29 inhibited adhesion of platelets by 78-88% relative to non-coated PET surface. These coatings retained the anti-adhesion properties after incubation in PBS or surfactant solution for 7 days, suggesting that the star polymer architecture provided high polymer chain density on the surfaces to prevent adhesion of platelets as well as coating stability to prevent exposure of bare PET surfaces. The results indicate that star polymers can provide an effective approach to the preparation of high density polymer brushes on PET surfaces for anti-adhesion coatings against platelets.

Chapter 3 showed inhibition of bacterial adhesion as antimicrobial activities on the coated surfaces. The polymer coated surfaces of star-PHEMA and star-H71M29 were resistant to bacterial adhesion by 94-97% relative to non-coated PET as well as resisting platelet adhesion.

The hydrophobic arms in heteroarm star polymer increased the hardness of coating surface. These results indicate that heteroarm star polymer coating methods has a lot of possibility for application to various artificial organs as biomaterials. Many functional star polymers would be developed for various applications in the future.

Future prospects

Biocompatible Coating materials

In the past, the hydrophilic polymers and zwitterionic polymers which have bloodcompatible and antibiofouling function have been reported. These biocompatible polymers can be applied as functional segments in the star polymers used in this study. By selecting hydrophobic segments, various substrates can be coated easily with star polymers.

In addition, by introducing cell-adhesion peptides, star polymers with selective cell adhesion functions can be developed (Figure F-1).

Temperature-responsive coated surface

It is well known that poly(*N*-isopropylacrylamide) is temperature-responsive polymer which is hydrophilic at low temperature and hydrophobic at high temperature. Temperature-responsive star polymers can be obtained by using such a polymer.

Gene delivery

A new gene delivery vector can be developed by introducing poly((2-dimethylamino)ethyl methacrylate) (PDMAEMA) in to star polymers.

Bone cement materials

Poly(methyl methacrylate) (PMMA) has been used as a bone cement in clinical application, but mechanical strength and compatibility to bone tissues must be improved. By introducing PMMA and/or cell adhesion peptides into star polymers, a better bone cement can be obtained.

X-ray sensitizing imaging materials

Biocompatible polymers (ex. Poly(ethylene glycol) (PEG) and sugar) are known to prevent foreign-body reactions. In addition to use those polymers as arms, incorporating europium (Eu) atoms into the core of star polymers, X-ray sensitizing and /or imaging materials can be developed.

Table F-1. Design of star polymers in future prospects

Biocompatible coating materials	
Functional segments	Function
Poly(ethylene glycol methacrylate) (PEGMA)	Antithrombogenic, Antimicrobial
Poly(2-methacryloyloxyethyl phosphorylcholine) (PMPC)	Antithrombogenic, Antimicrobial
Poly(carboxybetaine methacrylate) (PCBMA)	Antithrombogenic, Antimicrobial
Poly(sulfobetaine methacrylate) (PSBMA)	Antithrombogenic, Antimicrobial
Poly(2-hydroxyethylmethacrilate)-*b*-Peptide (PHEMA-Peptide)	Antithrombogenic, Antimicrobial Selective cell adhesion
Poly(N-isopropylacrylamide) (PNIPAM)	Temperature-responsive Drug release Low temp. : hydrophilic High temp. : hydrohobic

Gene vectors	
Functional segments	Function
Poly((2-dimethylamino)ethyl methacrylate)(PDMAEMA) (Homoarm star)	Electrostatic interaction with pDNA (polyplex)
PDMAEMA (Heteroarm star)	Electrostatic interaction with pDNA (polyplex)

Bone cement materials	
Functional segments	Function
Poly(methyl methacrylate) (PMMA) (Homoarm star)	Strong aggregation
PMMA PNIPAM Peptiede (heteroarm star)	Strong aggregation Temperature-responsive Cell adhesion

X-ray sensitizing and/or imaging materials	
Functional segments	Function
Poly(ethylene glycol) (PEG)-Sugar chain (Homoarm)	Water solubility Targeting cancer cells

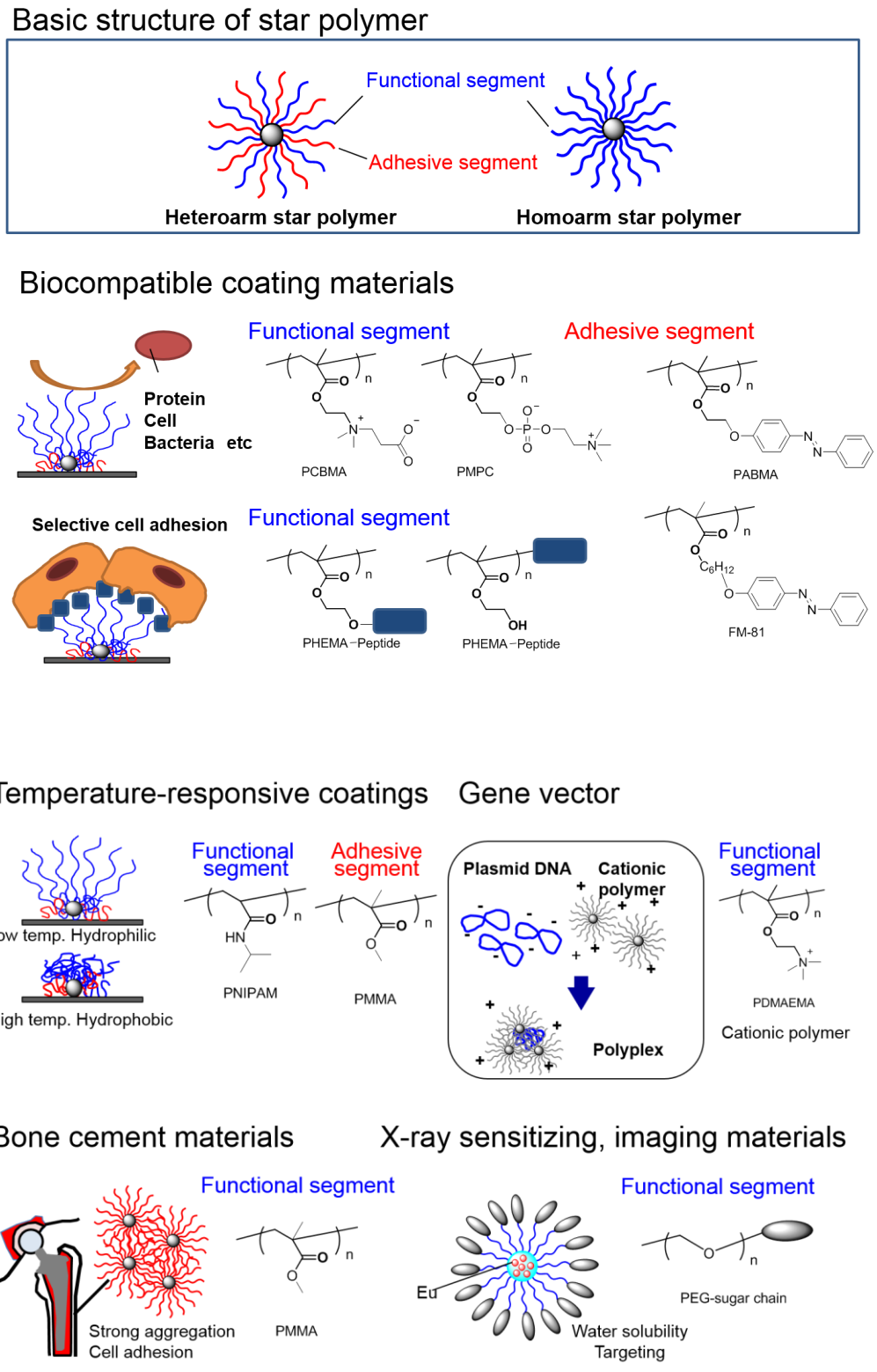

Figure F-1. Design and application of star polymers in future prospects

LIST OF PUBLICATIONS

The present thesis "Development of a new antithrombogenic and antimicrobial materials with heteroarm star polymer" is based on the following publications.

CHAPTER 1, CHAPTER 2 and CHAPTER 3

"Utilization of star-shaped polymer architecture in the creation of high-density polymer brush coatings for the prevention of platelet and bacteria adhesion"

Masayasu Totani, Tsuyoshi Ando, Kayo Terada, Takaya Terashima, Ill Yong Kim, Chikara Ohtsuki, Chuanwu Xi, Kenichi Kuroda, Masao Tanihara. Biomaterials Science, 2014, published."

RELATED PUBLICATIONS

“Inhibition of Biofilm Formation by Heteroarm Star Polymer Coatings”

Masayasu Totani, *Tsuyoshi Ando, Xiuwan Lan, Jianfeng Wu, Chuanwu Xi, Kayo Terada, Kenichi Kuroda,Masao Tanihara*

Macro/NAIST Joint Workshop for Emerging Researchers. (2012)

ACKNOWLEDGEMENTS

The studies in this thesis were carried out under the direction of Professor Masao Tanihara at the Graduate School of Materials Science of Nara Institute of Science and Technology (NAIST), Japan. The author expresses his sincere gratitude to Professor MasaoTanihara for his continuous encouragements and valuable advices all through these studies. Grateful acknowledgements are due to Professor Michiya Fujiki, Professor Jun-ichi Kikuchi, Associate Professor Tsuyoshi Ando, Assistant Professor Shiho Hirohara, and Assistant Professor Kayo Terada, Assistant Professor Mime Kobayashi of the Graduate School of Materials Science of NAIST for their helpful discussions and suggestions.

The author is deeply grateful to Assistant Professor Kenichi Kuroda of the Dental School at University of Michigan for his useful comments and discussions on these studies and Assistant Professor Chuanwi Xi of Department of Environmental Health Sciences, School of Public Health, University of Michigan.

I would also like to thank Dr. Xiuwan Lan and Dr. Jianfeng Wu, Dr. Haruko Takahashi, and Ms. Laura Thoma at the University of Michigan for helpful discussion. I also thank Prof. Mitsuo Sawamoto for the use of the GPC-MALLS instrument at Kyoto University, Prof. Kazuma Yasuhara, Ms. Manami Tsukamoto at Nara Institute of Science and Technology for the use of the DLS.

Sincere appreciations are due to Mr. Fumio Asanoma for their advices to measure ^{1}H NMR spectra. Great thanks go to Mrs. Yumiko Shinohara, Dr. Hidetaka Hougaku, Kinuyo Nishiyama and graduate students of the Biocompatible Materials Science Laboratory of NAIST for their supports. Finally the author is profoundly grateful to his family, Yoshio and Tomoko Totani, Ken and Satomi Nakano, Atsuko Nakano, Tomiko Yamamoto, his wife Kuniko Totani, his children Mio and Yui Totani for their care and encouragement.

June 2014

Masayasu Totani